ROCK PHYSICS MODELS FOR CONSTRAINING QUANTITVE INTERPRETATION OF ULTRASONIC DATA FOR BIOFILM GROWTH AND DEVELOPMENT

By

FATHIYA MOHAMMED ALHADHRAMI

Bachelor of Petroleum and Natural Gas Engineering

Sultan Qaboos University

Muscat, Oman

2009

Submitted to the Faculty of the
Graduate College of the
Oklahoma State University
in partial fulfillment of
the requirements for
the Degree of
MASTER OF SCIENCE
May, 2013

ROCK PHYSICS MODELS FOR CONSTRAINING QUANTITVE INTERPRETATION OF ULTRASONIC DATA FOR BIOFILM GROWTH AND DEVELOPMENT

Thesis Approved:

Dr. Priyank Jaiswal

Thesis Adviser

Dr. Estella Atekwana

Dr. Eliot Atekwana

.

ACKNOWLEDGEMENTS

'Imagination is more important than knowledge'.

Albert Einstein

By the support and strength given to me by Allah SWT, this work is finally documented. However, this thesis research would not have been accomplished without the support of many people. Foremost, I would like to express my thanks to Exxon mobile for supporting and funding my studies. I would like to express my sincere gratitude to my advisor Prof. Priyank Jaiswal for his continuous support during this work and research, for his patience, motivation, enthusiasm, and immense knowledge. His guidance helped me in all the time of research and writing of this thesis. I could not have imagined having a better advisor and mentor. Besides my advisor, I would like to thank the rest of my thesis committee: Prof. Estella Atekwana, and Prof. Eliot Atekwana, for their encouragement, insightful comments, and great questions. At times of desperation and when I felt almost quitting this work, they were there for me. My sincere thanks also go to all the great people at IIE and IIIS office, without you guys I wouldn't be able to complete my graduate studies. Likewise, many thanks go to Caroline A. Davis, PhD, for providing us with the required data essential to perform this work. Moreover, many thanks go to my friend Samiya Al-Balushi, Dr. Jack Dvorkin and Dr. Tiziana Vanorio for assistance with the rock physic modeling. In addition, I would like to thank Pride Abongwa for helping me with the Geochemistry analysis. I thank my fellow classmates in Oklahoma State University: for the stimulating discussions, for the sleepless nights we were working together before deadlines, and for all the fun we had together. In addition, I have been very privileged to get to know and to collaborate with many other great people who became friends over the last years. Thanks to all my friends for believing in me and filling my time with joy and happiness. I also would like to express my love and gratitude to my beloved family for their understanding & endless love through the duration of my studies. My genuine appreciation goes to my sister Munira for the inspirational quote she told me about. I always went back to it to get inspired and that's why I decided to write it at the first page of this work. Last but not the least; I would like to thank my mother, for giving birth to me at the first place and supporting me spiritually throughout my life

Name: FATHIYA M. ALHADHRAMI

Date of Degree: MAY, 2013

Title of Study: ROCK PHYSICS MODELS FOR CONSTRAINING QUANTITVE INTERPRETATION OF ULTRASONIC DATA FOR BIOFILM GROWTH AND DEVELOPMENT

Major Field: GEOLOGY

Abstract: This study examines the use of rock physics modeling for quantitative interpretation of seismic data in the context of microbial growth and biofilm formation in unconsolidated sediment. The impetus for this research comes from geophysical experiments by Davis *et al.* (2010) and Kwon and Ajo-Franklin *et al*. (2012). These studies observed that microbial growth has a small effect on P-wave velocities (V_P) but a large effect on seismic amplitudes. Davis *et al.* (2010) and Kwon and Ajo-Franklin *et al*. (2012) speculated that the amplitude variations were due to a combination of rock mechanical changes from accumulation of microbial growth related features such as biofilms. A more definite conclusion can be drawn by developing rock physics models that connect rock properties to seismic amplitudes. The primary objective of this work is to provide an explanation for high amplitude attenuation due to biofilm growth. The results suggest that biofilm formation in the Davis *et al*. (2010) experiment exhibit two growth styles: a loadbearing style where biofilm behaves like an additional mineral grain and a non-loadbearing mode where the biofilm grows into the pore spaces. In the loadbearing mode, the biofilms contribute to the stiffness of the sediments. We refer to this style as "filler." In the non-loadbearing mode, the biofilms contribute only to change in density of sediments without affecting their strength. We refer to this style of microbial growth as "mushroom." Both growth styles appear to be changing permeability more than the moduli or the density. As the result, while the V_P velocity remains relatively unchanged, the amplitudes can change significantly depending on biofilm saturation. Interpreting seismic data from biofilm growths in term of rock physics models provide a greater insight into the sediment-fluid interaction. The models in turn can be used to understand microbial enhanced oil recovery and in assisting in solving environmental issues such as creating bio-barriers to prevent water contamination or CO_2 leakage.

TABLE OF CONTENTS

Chapter Page

LIST OF TABLES

Table Page

LIST OF FIGURES

Figure Page

CHAPTER I

INTRODUCTION

1.1 Background:

Microorganisms organisms play an important role in changing environmental and hydrodynamic of porous media due to the development of microbial biomass (Brovelli *et al*., 2008). In porous media (e.g., subsurface soil or rocks), biofilm growth within the pore space can induce substantial modifications to rock mechanical properties and dynamics on a much larger scale. Microbial communities can grow and block a large fraction of pore space and effectively reduce permeability; the process is known as bioclogging (Taylor and Jaffe, 1990; Lappan and Fogler,1996; Bouwer *et al.,* 2000; Dunsmore *et al*., 2004). The ability to manage artificial and natural bioclogging and monitor microbial growth is essential in many applications. Microbial enhanced oil recovery (MEOR) is one of the applications where understanding bio-mass production is important for the process of extracting trapped oil in reservoirs and improving oil recovery (Zajic *et al*., 1983; Yen, 1990).

In addition, bioclogging treatments have been proven to be efficient in forming bio- barriers to control subsurface contamination plumes and at the monitoring of bio-barriers for CO_2 sequestration operations (Figure 1) (Pintelon *et al*., 2012).

The ability to resolve subsurface microbial growth with high spatial resolution is hindered by the capability to understand how microorganisms change their physical and chemical environment during the cell growth and biofilm development process. Many studies discussed the capability and potential of geophysical methods such as seismic and electrical techniques to compromise noninvasive option to detect, characterize and/or quantify the spatial distribution of biogeochemical processes (Williams *et al*., 2005; Atekwana *et al*., 2006; dejong *et al*., 2006; Atekwana and Slater, 2009; Slater *et al*., 2009). Geophysical methods have potential to detect and image biofilms formation in many applications such as microbial attachment/transport studies, imaging zones of bioclogging, soil remediation of liquefaction during earthquakes, and microbial enhanced oil recovery (Abdel Aal *et al.*, 2004-2006; Karatas, 2008; Williams *et al*., 2009; Ntarlagiannis *et al*., 2005-2007).

Geophysical techniques can help in monitoring microbial processes in porous media (Hubbard *et al*., 2008; Williams *et al*., 2008) because changes induced by biofilm formation manifest as geophysical anomalies. Here, the intrinsic assumption is that bio-changes depend on the rheological properties of the porous medium and fluids that are contained in the pore spaces (Li *et al*., 2001). For instance, geophysical methods based on acoustic wave propagation particularly in the ultra- sonic frequency range seem to be the most efficient to assist microbial imaging and help in monitoring microbial process in porous media. By-products of microbial growth such as biogenic gas (e.g., Williams,

2002) and mineral (e.g., Williams *et al*., 2005; dejong *et al*., 2006), can change the elastic properties of unconsolidated sediments (e.g., Davis *et al*., 2009 and 2010).

1.2 Case study:

Davis *et al.* (2010) presented time-lapse arrival time and amplitude data from a physical-scale experiment involving biofilm growth in unconsolidated sediments (Figure 2). Davis *et al.* (2010) observed that amplitudes and arrival times varied during the biofilm development and growth in the biostimulated column (Figure 3). Nearly 80% decrease in amplitude was recorded in the biostimulated column, raising up the question if P-wave attenuation (in ultrasonic frequency) is a positive indicator for biofilm formation. On the other hand, only ~2% increase in arrival time (~1% change in V_P) was observed in the experiment.

The scanning electron microscope (SEM) images obtained by Davis *et al*. (2010) showed apparent differences in the morphology of attached biomass between different regions (Figure 4). Accordingly, Davis *et al*. (2010) suggested that heterogeneity in the acoustic measurements from the biostimulated column are due to existence of more than one biofilm growth style. On similar lines, Kwon and Ajo-Franklin . (2012) conducted experiments which involved stimulating the production of the biopolymer dextran inside a column of sand while monitoring changes in permeability and seismic response using the ultrasonic pulse transmission method. In their attempt to check the feasibility of using increased attenuation as a proxy for decreased permeability, Kwon and Ajo-Franklin . (2012) recorded the same results observed in Davis *et al*. (2010) (Figure 5).

Davis *et al*. (2010) and Kwon and Ajo-Franklin . (2012) suggested the rock matrix properties such as porosity and permeability change due to biofilm development and thus explained the variation in their seismic data. The Davis *et al.* (2009;2010) study speculated that the P-wave attenuation could have occurred due to squirt flow and scattering, whereas the Kwon and Ajo-Franklin (2012) related the P-wave attenuation to a flow-induced loss mechanism related to the combined grain/biopolymer structure. A model that relates the effect of biofilm growth on seismic responses is lacking. This work demonstrates the development of biofilm growth models based on rock physics relations to explain the time-lapse geophysical data from Davis *et al*. (2010).

1.3 Objective of the work:

The objective of this research is to develop a rock physics model to explain seismic data obtained from the Davis *et al*. (2010) experiment. First, however, the rationale for using rock physics is needed. Rock physics draws a relationship between the geophysical data and rock properties. The sensitivity of seismic velocities to critical rock parameters, such as porosity, pore fluid type, saturation, and permeability, has been recognized for many years (Han and Batzle, 2004). Yet, the practical need to quantify geophysical data-to-rock-property transformations and their uncertainties has become critical over the past decade (Takahashi *et al*., 2000). For instance, rock physics modeling is used to interpret amplitudes for hydrocarbon detection, reservoir characterization, and reservoir monitoring (Teng, 1998). Discovering and understanding the seismic-to-reservoir relations has been the focus of rock physics research. In this paper rock physics are used to quantify microbial growth, biofilms formation, and byproducts in porous rocks.

Several studied have been conducted to quantify and interpret seismic data by means of rock physics in different environments such as carbonate rocks, mud rocks and gas hydrates (Nur and Dvorkin, 2003-2004; Dai *et al.*, 2004). I propose that biofilm can be modeled much like hydrates as biofilm saturation is time dependent precipitate from pore fluid. None of the previous rock physics models considered or have incorporated the effects of microorganisms. Thus this study is attempt to model seismic attributes and seismic response alterations due to microbial growth by means of rock physics models. Rock physics models have the potential to (1) provide explanations for the results obtained by seismic methods, thus helping in testing and validating of bioclogging models and numerical simulations used for assessing microbial induced changes on flow and transport properties and (2) be used for evaluating and monitoring spatial or temporal variations in seismic attenuation due to biomass distribution in subsurface environments (e.g., microbial enhanced oil recovery (MEOR), and engineered bio-barriers).

By developing a rock model, I expect to a) quantifying microbial growth styles and structures; b) construct biofilm saturation profiles that can be related to the changes in seismic amplitudes using rock physics models; and c) provide a tool to the science database to infer the rock microstructure from velocity profiles. The rock physics models that relate seismic data such as acoustic velocity and attenuation to hydraulic changes in the media can be useful in elucidating the effect of biofilm formation on seismic properties and may be an effective tool in monitoring microbial growth and permeability alterations.

CHAPTER II

TYPE TITLE HERE

2.1 Davis *et al*. (2010) Experiment

In this research, time-lapse arrival time and amplitude data from Davis *et al*. (2010) are used to model the effect of biofilm growth on seismic velocities and seismic waves attenuation. In the Davis et al. (2010) experiment, bacterial growth was stimulated over a period of 26 days (17^{th} June to 11^{th} July). Nine set of ultrasonic waveforms scans were recorded at an interval of 2 – 4 days. Individual set of scan comprise ultrasonic measurements at 168 locations (a rectangular matrix of 14 X 16 cells). Although data reported by Davis *et al*. (2010) are not uniform temporally, they adequately captured the bio-stimulation character in terms of biofilm inception, growth and decay. In the experiment, the ultrasonic waves between source and receivers travelled through three different media – water, glass (Pyrex) enclosure, and bio-stimulated sediments. To discount for traveltime in water (5 mm or either side) and Pyrex (2 mm on either side), at the outset we apply a constant shift of 7.7 ms to the arrival times. We convert the resulting traveltime dataset to velocity assuming straight rays in 51mm thick sedimentary column.

Travel times were converted to velocity and discover two dominant time-lapse trends – continually increasing and continually decrease (Figure 6). Velocity model from straight-ray tomography models showed a fairly random distribution of high and low velocity patches in the first 7 days. From Day 10 onwards, a vertical zone of low velocity starts appearing in the center. We speculate that this zone is weak and of higher porosity which is more conducive to fluid flow. This gradual change in porosity could be as a result of preparation of the sample box or due to the growth of biofilms. Analysis of the velocity data suggested that biofilms exhibited different impact on the sand stiffness frame work in different regions. The velocity started on Day 1 with a value of 1.711 (km/sec) and over the course of the experiment, different patches of high velocities along with patches of low velocity. Tracing two different spots that had different changes in velocity with time, distinct behaviors for the acoustic velocities were observed (Figure 7). Position A presented an increase of up to 1.8 (km/sec) in velocity values due to biofilm growth and formation; whereas, position B showed a decrease in velocity up to 1.65 (km/sec) with time due to biofilm production. Even though the change in velocity values was negligible, the desire to find a technique that can be used to explain these two opposite behaviors was raised at this stage.

We infer from the Davis *et al*. (2010) work that the change in biofilm growth styles might be the main cause for changes in the acoustic properties. However, the drop in pH value in the biostimulated column presented by Davis *et al*. (2010) suggested the possibility of metabolic byproducts such as dissolved gas to be one of the reasons for changes in the acoustic properties. In this work, the effects of both bio-product (biogenic

gas) and biofilm growth styles on seismic data during microbial growth and biofilm development in unconsolidated sediment were investigated using rock physics models.

2.2 Rock Physics Modeling Basic

Rock physics models are used for quantitative characterization of geophysical measurement such as seismic acoustic data. Rock physics models help to address the relationship between elastic parameters made from surface and subsurface rock properties and mineralogy. Rock physicists find the relationship between material properties and the observed seismic response, and thus create a predictive model so that these properties may be detected seismically. For given formation composite and pore fluids, using rock physics can help find velocity, density, and their relationships to porosity and elastic moduli (bulk modulus) (Johnston *et al*., 1995; Mavko, 2002).

2.2.1 Defining the Matrix, Fluids and Placement of Additional Components

From a rock physics perspective, the rock is divided into two parts – the solid frame, which comprises the mixture of minerals (matrix) and the pore fluid, which comprises mixture of fluids such as gas, oil and water (Wang, 2001). Any additional component (such as the biofilm) to the system must be defined as either being part of matrix or part of the fluid. Therefore, constructing synthetic elastic models of the rock involves four steps: (1) defining the matrix, the fluids, and the location of the additional component if one or more exist; (2) assembling and constructing a dry rock matrix modulus; (3) analyzing pore fluid separately and determine its modulus as well and (4) introducing fluids into the dry matrix and reuniting both modulus in one effective system modulus via the Gassman's relationship (Figure 8) (Gassmann, 1951).

2.2.2 Assembling and Constructing a Dry Rock Matrix Modulus

For simplicity, in this work it is assumed that the rock matrix is comprised only of quartz and the pore-fluid is simply water. The bulk modulus of the individual solid and fluids are known from literature and their values listed in (Table 1). Batzle and Wang (1992) relations were used to correlate fluid properties with temperature and pressure to calculate densities and the bulk modulus of the fluids. For modeling purposes, a homogenous background system was assumed of matrix composed of quartz grains that are not cemented, spherical or randomly packed. For spherical unconsolidated sediment the bulk (K_{HM}) and shear (G_{HM}) moduli of dry rock is expressed as:

$$K_{HM} = \left[\frac{n^2(1-\varphi_c)^2 G^2}{18\pi^2(1-\nu)^2} P\right]^{\frac{1}{3}}, G_{HM} = \frac{5-4\nu}{5(2-\nu)}\left[\frac{3n^2(1-\varphi_c)^2 G^2}{2\pi^2(1-\nu)^2} P\right]^{\frac{1}{3}} \quad (1)$$

These equations are known as Hertz-Mindilin relations and they describe moduli at the critical porosity Øc, which is the porosity at which the solid particles just flow in the fluids, thus presenting the elastic moduli at the critical porosity endpoint, where n is average number of contacts per grain for unconsolidated sediment for which we use n of 6. P, the effective pressure (delta between the pore pressure and the overburden pressure) and v and G are the Poisson's ratio and shear modulus of the solid phase.

The other end member is representing elastic moduli at zero porosity where we just have the mineral phase. That can be determined by the average and mass balance relationships (Hill, 1952):

$$\begin{aligned} K_S &= 0.5 \cdot \left[\sum_{i=1}^{m} f_i K_i + \left(\sum_{i=1}^{m} f_i / K_i\right)^{-1}\right], \\ G_S &= 0.5 \cdot \left[\sum_{i=1}^{m} f_i G_i + \left(\sum_{i=1}^{m} f_i / G_i\right)^{-1}\right], \\ \rho_S &= \sum_{i=1}^{m} f_i \rho_i, \end{aligned} \quad (2)$$

Where K_s, G_s, and ρ_s are the bulk and shear moduli and density of the mineral (solid) phase, respectively; m is the number of the mineral components; f_i is the volumetric fraction of the i-th component in the solid phase; and K_i, G_i, and ρ_i are the bulk moduli, shear moduli and density of the i-th component respectively.

At porosities other than zero and critical porosity, many mathematical models are introduced to connect those two end members. The two end members include trajectories corresponding to the upper and the lower Hashin Shtrikman bounds. The upper bound assumes that a softer mineral/fluid is enclosed in a stiffer shell. The lower bound (applicable in this case) assumes *vice-versa*. In this work, referring to all the data provided by Davis *et al*. (2010) especially the ESEM images, and knowing that hosting media for the

was unconsolidated rock, the lower Hashin Shtrikman bound was used to connect the two end members (Figure 9) (Dvorkin and Nur, 1996).

2.3 Biofilm Growth Styles

Using the SEM image, Davis *et al.* (2010) observations confirmed microbial cell attachment to sand surfaces and observed different biofilm structures in different zones. In this paper, this information was utilized in creating the rock physics models. In order to introduce any new components to the rock system such as biofilm in this work, this new composite can either be considered as part of matrix or as part of the fluids. However, biofilm attached to sediment presents unique challenges as biofilm can be attached with the sediment in many complex ways. Biofilm needs a solid to attached to in order to develop its network of bio-cells (Bendaoud *et al*., 2011).

The biofilms are introduced in our system with two different fates. However, their

initiation is the same. At their inception, we assume that the biofilm forms a continuous layer on the grain surface. In the rock physics model, we conceive this layer as the base phase (Figure 10a). As the biofilm saturation increases, the bioflims can continue to "fill" spaces or, wherever there is space available for the EPS material to expand (such as the pore space, grow into the pores taking the shape of a "mushroom" (Figure 10b). (Picioreanu *et al*., 2010). In a "filler" mode, the biomaterial is considered to be embedded as part of the host rock matrix and bears the load (Figure 11a). The mushroom style, on the other hand, grows and builds up in a non-continuous style. As biofilm exists in pore space, the EPS material will have more space to expand and thus create an apparent low density texture with high porosity. This part of the biofilm will grow as an extended surface freely floating in pore spaces where fluid exist (Figure 11b). This growth style is non-loadbearing, i.e., biofilm do not participate in transferring the seismic stress. Translating the two growth styles into rock physics models means that the two end members of mineral phase and critical porosity will be combined using the filler model and mushroom model depending on where the biofilm is considered to be in the sediment.

2.3.1 Loadbearing "Filler" Model

Considering biofilm as part of the mineral frame, a loadbearing model can be introduced to simulate synthetic seismic elastic velocity. To quantify this effect, first, biofilm saturation of the pore space S_b is presented, which means the biofilm volume in a unit volume of rock compare to the total porosity of the mineral frame φ_t. Therefore, the mass of biofilm per unit volume of rock is:

$$C_b = \varphi_t S_b \tag{3}$$

Accordingly, the porosity available for fluid $\bar{\varphi}$ after biofilms (fills part of the pore space) becomes part of the solid is:

$$\bar{\varphi} = \varphi_t - C_b = \varphi_t(1 - S_b) \tag{4}$$

$\bar{\varphi}$ is equivalent to φ_t for S_b = 0 and $\bar{\varphi}$ is zero for S_b = 1. The volume fraction of biofilm in the new solid phase where biofilm is part of the matrix is:

$$C_b/(1-\bar{\varphi}) = \varphi_t S_b/[1-\varphi_t(1-S_b)] \tag{5}$$

To calculate the elastic moduli and density of the new solid phase material that includes biofilm, Hill's average relations are used. But instead of the original f_i, the new volume fractions are used which consider the biofilm as being part of the solid. Hence, the modulus at the end member where there is no porosity or where there is total mineral phase is determined.

To calculate the other end member at the critical porosity modulus, the Hertz-Mindilin relation presented previously is used. The next step is to connect these two endmembers and build the dray effective modulus. As this work evaluated the lower Hashin bound, the two end members can be related as (Dvorkin and Nur, 1996):

$$\begin{aligned} K_{Dry} &= \left[\frac{\varphi/\varphi_c}{K_{HM} + \frac{4}{3}G_s} + \frac{1-\varphi/\varphi_c}{K_s + \frac{4}{3}G_s}\right]^{-1} - \frac{4}{3}G_s, \\ G_{Dry} &= \left[\frac{\varphi/\varphi_c}{G_{HM} + Z} + \frac{1-\varphi/\varphi_c}{G_s + Z}\right]^{-1} - Z, \\ Z &= \frac{G_s}{6}\left(\frac{9K_s + 8G_s}{K_s + 2G_s}\right). \end{aligned} \tag{6}$$

The bulk modulus of the pore fluid (water in this case) K_f can be calculated using Ruess bound:

$$K_f = [S_w/K_w]^{-1} \tag{7}$$

Where S_w is water saturation and K_w is water's bulk modulus. Fluid density ρ_f is calculated by:

$$\rho_f = S_w \rho_w \tag{8}$$

To introduce the fluid to the dry effective modulus we used Gassmann equation (Gassmann, 1951) for saturated rock moduli which is expressed as:

$$K_{Sat} = K_s \frac{\varphi K_{Dry} - (1+\varphi)K_f K_{Dry}/K_s + K_f}{(1-\varphi)K_f + \varphi K_s - K_f K_{Dry}/K_s}, G_{Sat} = G_{Dry} \tag{9}$$

Where the bulk density ρ_b is obtained from mass balance as:

$$\rho_b = (1-\varphi)\rho_s + \varphi\rho_f \tag{10}$$

Finally, V_p and V_s can be computed using the elastic moduli K_{sat} and G_{sat} and density ρ_b as:

$$V_p = \sqrt{\frac{M_{sat}}{\rho_b}}, \quad V_s = \sqrt{\frac{G_{sat}}{\rho_b}} \quad \text{and} \quad M_{sat} = K_{sat} + \frac{4}{3}G_{sat} \tag{11}$$

2.3.2 Non-loadbearing "Mushroom" Model

A different approach towards modeling the elastic properties of sediment with biofilm is to assume that the biofilm is not totally part of the solid or all suspended in the

pore fluid. As an alternative, part of the biofilm is attached to the matrix and the extension occurs in the fluid. In this case, the biofilm will not act to change the bulk modulus of the matrix or the pore fluid; instead, it will have an effect on the densities, altering the overall density of the mineral frame and the pore fluids. The assumption is that once the biofilm already exists in the system attached to a solid particle, and has the right environment and nutrient to grow, it starts developing around the solid particle, evolving as a head-tail like fragment as mentioned in some microbial structure analysis studies (e.g., Klapper *et al*., 2002).

Mushroom body shape is the closest mimic of this biofilm growth style (Figure12). The head part will have role in changing the density of the sediment. As a thin sheet of biofilm already coats the grain and is attached to solid sand particles, the biofilm will grow creating the tail structure with many associated pores. This tail part of the biofilm will be freely floating in the pore fluid, causing some density variation due to contact with water. This implies that each part of the biofilm body (head and tail) will have different densities and impact on the surrounding environment.

Therefore, to calculate the bulk modulus at zero porosity or at the mineral phase, the biofilm is not considered as part of the solid. Accordingly, original Hills (1952) average equations presented earlier can be used to compute the bulk and shear modulus of the solid. However, in calculating the solid density, the influence of biofilm must be considered. Hence, the volume fraction of biofilm which will be presented by the saturation of biofilm at head stage only S_{b1} must be added to the density ρ_{b1} of the head biofilm. Thus, the total solid density ρ_s in this case is:

$$\rho_s = f_{quartz}\rho_{quartz} + S_{b1}\rho_{b1} \quad (12)$$

To present the end member at critical porosity Øc, the Hertz-Mindilin modulus relation is used. Following will be joining the two end members by means of the lower Hashin-Shtrikman bound (Dvorkin and Nur, 1996). For the pore fluid bulk modulus K_f of water in this case Ruess equation is used keeping in mind not to consider the biofilm as being part of the fluid. However, while computing the total fluid density ρ_f , the biofilm must be considered with volume fraction equivalent to biofilm saturation higher than the saturation of biofilm needed to create the head part S_{b2} and thus the biofilm has a density of ρ_{b2} . Total fluid density can be expressed as:

$$\rho_f = S_w\rho_w + S_{b2}\rho_{b2} \quad (13)$$

Next, is obtaining saturated rock modulus by Gassmann relations and then calculating the seismic elastic compressional and shear velocities.

2.4 Porosity Estimation

Researcher such as Sakurada *et al*., (1962); Yamanaka *et al*., (1989); Nishi *et al*., (1990); Tajima *et al*., (1995); Stoodley *et al*., (1998-2002); Horn *et al*., (2002); Klapper *et al*., (2002); Astley *et al*., (2003); Guhados *et al*., (2005); Hsieh, (2008); and Aggarwal and Hozalski,(2010) have measured the mechanical properties of bacterial cellulose (Table 2). For molding purpose in this study, the biofilm moduli was taken as average values from Table 1 - 0.18 MPa for K and 0.67 KPa for G for *Pseudomonas aeruginosa* biofilm was used.

The first step in modeling Davis *et al.* (2010) time-lapse data is to determine biofilm-free porosity. V_P on Day 1 is 1.711±0.0051 km/sec. Assuming the matrix to comprise pure quartz and pore fluid to comprise water, Helgerud's model yield initial system porosity as 37.85%. To estimate a porosity value for the biostimulated sand column, a synthetic model by means of rock physics was constructed. The biostimulated column was modeled as a system of sand and water assuming that the background composite is quartz (100%). The process was done by building a dry effective rock model and then adding fluid into the pores. Basically, adding biofilm to the sand column as an extra component caused reduction in porosity with time. The bulk modulus of the saturated rock system was determined and, therefore, velocity was estimated. The change in velocity due to microbial growth was obtained. With the knowledge of the background velocity and initial porosity biofilm saturation can be estimated from the time-lapse velocity data after assigning a particular growth model to a particular cell (Figure 13).

2.5 Velocity Changes Due to Dissolved Gas

As discussed earlier when analyzing the Davis *et al*. (2010) data set, dissolved gas was suggested to be a possible reason for the change in the acoustic properties. In the *Davis et al.* (2010) experiment, the pH values measured for the control column remained steady near a pH value of 7 throughout the experiment. However, the pH values measured from the biostimulated column gradually decreased from pH value of 7 to near 4.4, and remained at a pH of 4.4 to the end of the experiment (Figure 14). For the pH value of water to drop from a value of 7 to 4.4, the alkalinity of the water must have changed. As reported in Davis *et al*. (2010) this increase in acidity was thought to be a result of accumulation of waste products due to biofilm detachment and cell death. Acidity

increase can be presented by an increase in the amount of dissolved bio-organic gas in the fluid. The expected resulting gas from bio-product is CO_2 which can dissolve in water to form carbonic acid:

$$CO2 + H2O \leftrightarrow H2CO3 \tag{14}$$

Carbon dioxide gas will be modeled in the system according to the *Le Châtelier* principle that states that if a reaction is at equilibrium and conditions are altered so as to create a new *equilibrium state*, then the composition of the system will tend to change until a new state of equilibrium is attained (Le Chatelier, 1898).To test how much the alkalinity of the water has been changed to the degree that caused a drop in pH values from 7 to a value of 4.4, *Henry's* law was used (Smith and Harvey, 2007):

$$\log P_{CO2} = -pH + \log\left(\frac{M_{HCO_3^{-2\gamma}} CO_3^{-2}}{KCO2Kl}\right) \tag{15}$$

Where: pH=-log [H+].

Here $M_{HCO_3^{-2\gamma}} CO_3^{-2}$ are the activity coefficient and the molarity respectively. K_1 is the first dissociation constant of H_2CO_3, and K_{CO2} is Henry's law constant for $CO_{2(g)}$; both values are corrected to the temperature (T) of the sample. The evaluated values of $\log P_{CO2}$ using Phreeq-C geochemical model software are presented in (Table 3), and in (Table 4) they were converted to $P_{CO2}\left(\frac{mol}{liter}\right)$ values which represent the amount of dissolved CO_2 gas in water for different alkalinity of water under the room temperature and pressure mentioned in Davis *et al.* (2010).

P_{CO2} values are equivalent to the gas to water ratio (GWR) which is the amount of gas in mol per liter of water. This ratio enters in the calculations of bulk modulus of water (K_{water}) in the rock physics models. K_{water} is consider as a very important fluids property to calculate bulk modulus of total fluid K_{fluid} and thus bulk density (Batzle and Wang, 1992). Therefore, adding dissolved gas to the fluid in the rock system used in Davis *et al*. (2010) is going to influence the calculation of fluid properties which, in turn, will affect the calculation of compressional velocity that depends on both bulk density and K_{fluid}.

2.6 Velocity Changes due to Microbial Growth

Using the two rock physics models described above, the biofilm saturation changes were modeled in loadbearing mode and a relation of change in velocity due to increasing in biofilm saturation S_b was plotted (Figure 15a). On the other hand, microbial growth in mushroom arrangement was modeled as well and V_P was plotted with increasing S_b (Figure 15b). Velocity changes with respect to the velocity on Day 1 were used to map the velocities to saturation. The difference in velocity ΔV was calculated for all zones in the 2-D scan section as $\Delta V=V_n-V_o$, where V_n is velocity in day n and V_o is the initial or day 1 velocity. If ΔV presented a positive value which indicates an increase in velocity, the zone was assigned to be accumulated with loadbearing growth style biofilm. However, if ΔV resulted in a negative value which represented a decrease in velocity compared to day 1, the mushroom growth style of biofilm was assigned to that zone. Otherwise, if ΔV value was zero, no change in velocity occurred and thus no biofilm was presented in this zone. By this classification technique, the types of biofilm growth styles were classified for each zone. Using these classification profiles and the

synthetic velocities obtained previously, the velocity tomography profiles was converted into biofilm saturation profiles.

2.7 Attenuation due to Microbial Growth

To explain the attenuation data, a large amount of work done on seismic wave attenuation in geological media was reviewed. For example, the work done by Winkler *et al*. (1979); Mavko *et al*. (1979); Winkler and Nur (1980); Winkler and Nur (1982); Walsh (1995); Gurevich *et al*. (1997); Roth *et al*. (2000); Carcione and Picotti (2006); *Maultzsch et al.* (2007); Gurevich and Ciz (2006); Adam *et al*. (2009); Muller *et al*. (2010); Gurevich *et al.* (2010) and Masson and Pride (2011) allows for conclusion that attenuation is a fundamental property of partially saturated rocks. In general attenuation is the decay in amplitude of the seismic wave as it propagates in space and time. None of the two authors mentioned above have adopted the same mechanism for modeling attenuation. This says that the relationship between the seismic attenuation and rock properties is very complex. Many factors affect seismic wave attenuation such as pore structure, fluids content, and connectivity of pore, mineral composition and fractures (Boadu, 1997; Babaia, 2000).

In this thesis attenuation is measured using dimensionless quantity called the Q factor (energy of seismic wave/ energy dissipated per cycle) represented as:

$$Q = \frac{2\Pi E}{\Delta E} \tag{16}$$

Where E is the energy of the wave, and ΔE is the change in energy per cycle. To estimate Q from the given amplitude data, for a medium with linear stress-strain relation, it is known that wave amplitude A is proportional to E (Hedlin, 2004). Hence:

$$\frac{1}{Q} \alpha \frac{\Delta A}{\Pi A} \tag{17}$$

From which the amplitude fluctuations due to attenuation as can be obtained as:

$$\frac{1}{Q} = \frac{2\Pi A}{\omega A_0}$$

(18)

Where λ is the wave length and ω is angular frequency. Moreover, attenuation is measured by the decay of a plane wave as it propagates through a rock material as suggested by Boadu (1997) and is determined by:

$$A(x) = A_0 e^{ax} \tag{19}$$

Where A_0 is the initial amplitude of the propagating wave, A(x) is the wave amplitude at a distance x, and a is the attenuation coefficient mentioned in Boadu (1997). The attenuation coefficient a can be represented as:

$$a = 0.432 + 0.011\Phi + 0.002K - 0.003D + 0.251C \tag{20}$$

With Φ is the porosity (percent), K is the permeability (millidarcy), D is the mean grain size (mm) and, C is the clay content (percent).

For this rock system, Φ=35%, D=0.6–1.18 mm from Davis *et al*. (2010), and clay content= zero. Permeability is the measure of the soil's ability to permit water to flow through its pores or voids, and it will be affected by the microbial growth and biofilm development.

Substituting equation (19) into (18) and resulted in:

$$\frac{1}{Q} = \frac{A_{o2}^{eax} - A_{o1}}{A_{o1}} = (A_{o2}^{eax} - 1) \quad (21)$$

Attenuation and permeability were the only unknowns and were modeled with respect to microbial enhancement. To model attenuation by the given equation, permeability had to be increased for low biofilm saturation and then decreased with biofilm development (Figure 16). For attenuation modeling the peak to peak amplitude data is being used (Figure 17).

CHAPTER III

RESULTS & ANALYSIS

3.1 Velocity Changes Due to Dissolved Gas

There was a decrease in the velocity changes due to an increase in the amount of CO_2 gas dissolved in water presented as GWR in the rock physics model; however, the decrease was from 1.7075 to 1.704 (km/sec) for 100% dissolved CO_2 gas in the system. This decrease in velocity due to dissolve gas was not significant and was less than the decrease in velocity calculated from arrival time data.

3.2 Velocity Changes Due to Microbial Growth

Modeling biofilm in the loadbearing case produced an increase in V_p with increasing biofilm saturation S_b as shown in.On the other hand, by modeling biofilm in the mushroom arrangement, V_P decreased with increasing S_b. Only small changes in apparent velocity occurred, but consistent decreases and increases were observed from previous work conducted by Davis et al. (2010).

It was observed that to increase the V_P from initial value of 1.711 (km/sec) to 1.85 (km/sec), the biofilm saturation needs to be as high as 45%. This increase due to loadbearing growth style was reported to be remarkably insignificant, varying by a maximum of ~25 m/s or about 1-2%. This observation showed that the gel-like microorganisms do not affect the grain stiffness. Even though the decrease in velocity was insignificant, to decrease the velocity from the initial value of 1.711 to 1.65, as it is the lowest velocity value reported, the biofilm saturation in the pore space had to be close to or exactly 45% and could be as high as 65% in some pores.

Remarkably, the synthetic models of velocity matched the real data obtained from the velocity tomography generated earlier by the arrival time data. This suggested that biofilm introduced to the sample in the biostimulated column developed in both growths style. When classifying the growth styles of biofilm according to velocity changes as presented in (Figure 18), the mushroom growth style appeared to cover 60% of 2D-section as the biostimulated sand sample had high porosity of almost 35%, and was covered by more than one loadbearing growth style. Accordingly, the biofilm saturation distribution was obtained for each growth style and as shown the loadbearing model occurred almost at the center of the 2-D map; whereas the rest is the mushroom model. Some areas did not show any velocity changes, thus no microbial growth occurred at these locations. Toward the end of the experiment, the range of biofilm saturation was observed to vary between 0 to 65%.

3.3 Attenuation Due to Microbial Growth

When assembling the 2-D scan data set for amplitude changes due to microbial growth and development, the change in amplitude with respect to increasing biofilm saturation was observed for each growth style separately. If $\Delta A = 0$ is set as a reference line, the dominant growth style to cause an increase in amplitude is loadbearing. In addition, both growth styles a play part in causing the decrease in amplitude; therefore with an increase in attenuation, the mushroom style effect is more significant, as it covered more space compared to the loadbearing growth style.

Attenuation was modeled for the two different growth styles using the peak to peak amplitude data (Figure 19-20). Estimated attenuation was based on the squirt flow model that has been shown to be an important attenuation mechanism in rocks (Mavko et al., 1979; Murphy et al., 1986). The calculated inverse of the quality factor Q^{-1} as the ratio of change in amplitude with respect to the initial amplitude A_0 was modeled with respect to permeability modifications. As it was assumed in Kwon and Ajo-Franklin . (2012) study permeability was determined from Darcy's law (Brinkman, 1949), while assuming single-phase flow. It is observed that to model attenuation, permeability had to be increase at very early stages of biofilm growth for both growth styles. In this work, permeability was raised to a value of 0.6 millidarcy for 20% saturation of bioflm. Gradually, the permeability started to decrease due to attenuation alterations and to insoluble biomass formation. Attenuation responds for both growth styles presented virtually identical and parallel decreases and increases in attenuation in a cyclical manner such as the attenuation alteration produced earlier when testing the effect of biofilm growth on amplitude data.

CHAPTER IV

DISCUSSION

4.1 Major Patterns in the Observations

Previous studies such as Davis *et al*. (2010) and Kwon and Ajo-Franklin . (2012) attributed the observed amplitude variation in the biostimulated sample in their experiments to biofilm development and growth. This attribution was based on observations including SEM images of samples at locations with increased/decreased acoustic attenuation. This study has proposed rock physics models to explain Davis *et al*. (2010) data. The method could be potentially extended to explain Kwon and Ajo-Franklin . (2012) data but it is beyond the scope of the present study. One of the key features of this study is the examination of pH variation. The change in pH is attributed to metabolic byproducts and gas (mainly CO_2) that could have been formed through biofilm formation and decay. No free was reported during the observations of the experimental column of the work conducted by Davis *et al*. (2010) or Kwon and Ajo-Franklin . (2012). However, lowering of pH confirms that dissolved gas was present, which has been using GWR ratio in the rock physics models. As GWR increases from 0-100%, V_P decreases.

Within the framework of Davis *et al*. (2010) experiment only minimal (0.02 km/sec) velocity change was observed by introducing dissolved gas into the model, indicating that the effect of gas was insignificant in causing seismic data heterogeneity.

It was recognized from the results that the velocities changed in two dominant time-lapse trends – continually increasing and continually decrease. The continual trends can be explained using our models by respectively introducing biofilms as a part of dry sediments or fluids. However, we suspect that a large part of the Davis *et al*. (2010) model has both growth styles. Exact expressions of mixed systems is a matter of further research and which requires generation of more physical scale data such as those generated by Davis *et al*. (2010).

4.2 Justification for Data and Models

To justify the change in sediment modulus and microbial influence to the surrounding as biofilm formed, we have to know biofilm moduli. Previous works that attempted to study the rheology and mechanical properties of microbial substances outlined that the modulus of biofilm is very low compared to the modulus of sand (Watson *et al*., 1995; Stoodley *et al*., 1999-1998; Valls and de Lorenzo, 2002; Dunsmore *et al*., 2002; Allen *et al*., 2007; Hsieh, 2008; Bendaoud *et al*., 2011). Therefore, when merging biofilm and sand modulus together, the effect of bio-material on the sand stiffness will be minimal. Hence, the microbial-induced alterations on acoustic velocity will be insignificant.

Biofilm may alter the grain contact coupling; however, this depends on the location where biofilms are present in the sediment frame. Biomaterial that exist and grow in the pore space may cause a decrease in the volume and size of pores which alters the pore throat geometry, hence affecting seismic signal responses and an increase in

attenuation. This is especially true if the thin layer of biofilm which grows around the grains surrounding pore space where fluid already exists possess a kind of slipping effect for the fluid (Kraigsley *et al*., 2002). Thus, increasing fluids mobility are in fact represented as an increase in flow rate and a reduction in shear effect are found around the pores (Chellam, 1992). On the other hand, biofilm formations in the matrix can help in providing additional coupling and support among grains, thus stiffening the rock frame and decreasing attenuation (Davis *et al*, 2010).

To replicate time-lapse velocity data from the Davis *et al.* (2010) experiment, we formulate the two models with appropriate time-lapse saturation of bio-films. Results show that biofilmsaturation increases with time to a threshold value in both models following which they stay almost constant over the period of observation. The thresholds for both models are different. When bio-films are a part of fluid, the threshold can be as high as 80%. Independently, we model attenuation as a function of porosity, permeability, and grain size.

4.3 Permeability Expression in Bio-Contaminated System

The permeability model showed an increase in biofilm saturation of about 20% and then a decrease in bio-saturation to the end of the experiment. To elucidate permeability model, the overall permeability of the system first needed to be defined. Then the permeability is combined with the knowledge of biofilm growth styles to have a better understand of attenuation variations. The overall system permeability of the rock physics model can be expressed as the sum of rock and biofilm permeability (Figure 21).

$$K_{all} = K_{rock} + K_{biofilm} \quad (22)$$

Where K_{rock} is the rock system permeability that is presented by the original conductivity of the fluid in the system. $K_{biofilm}$ is the biofilm permeability which is representing the new fluid paths that are generated by bio-tubes and both permeability change with respect to the biofilm saturation. The concept of bio-tubes was introduced recently by Costerton (2008) who reported a few years ago that bacteria cells that form biofilms have little connections running between the cells, so that the jelly sticky material or what is referred to as the sitoplasma of one cell is in communication with the other cell in the bio-community. This opens channels of communication and creates biofilm permeability between the cells.

These bio-tubes will represent biofilm permeability $K_{biofilm}$ and the rock permeability K_{rock} can be expressed using Kozeny equation (Berryman and Blair, 1987; Shafahi and Vafai, 2009) as:

$$\mathrm{Krock} = \frac{\mathrm{Co}}{\mathrm{M}} \varepsilon^{3} \tag{23}$$

Where Co is a constant , ε^{3} factor is dependent on the porosity and decreases with reducing the system porosity and the specific surface, M, is:

$$\mathrm{M} = \frac{\mathrm{A}}{\mathrm{Vbulk}} = \frac{\Pi \mathrm{d}^{2}}{\alpha \mathrm{d}^{3}} = \frac{\Pi}{\alpha \mathrm{d}} \tag{24}$$

Where α is the arrangement packing factor for sphere grain shape, and d is the grain diameter, all these factors will change and effect K_{rock}. Due to biofilm growth surrounding the grains, the grain diameter is considered to increase and thus having influencing on permeability proportionally. However, the biofilm growth will reduce

porosity and will occupy some of the empty space in the system which will reduce permeability. The two permeability changes due to microbial growth and biofilm formation can be explained by relating the alteration to changes in biofilm growth structures and styles.

4.4 Permeability Changes in Bio-Contaminated System

The base phase occurs at a saturation less of than 20% in the early stages of biofilm formation (Figure 22). At this stage, a thin layer of EPS begins to cover the micro-organisms cells attached to sand grains, and forms a continuous thin sheet of biofilm around the grains as a base. As these thin sheets continuously grow and cover the sand grains, they form what is introduced in this study as connected bio-tubes. The bio-tubes absorb fluids through a porous medium and act as a fluid absorbing agent thus affecting the system permeability by creating new paths for fluids and connecting pore spaces. This will act to assists in increasing the mobility of fluids in the system by increasing $K_{biofilm}$. At the base stage when the grain are covered with these thin layers of biofilm, called base layers, these bio-layers surrounding the grain will increase the grain diameter, and thus the specific surface (M) value which is the will decrease causing an increase in $K_{rock.}$. As both biofilm and rock permeability increase, i.e., overall system permeability (K_{all}) will increase.

At biofilm saturation greater than 20%, the surface phase or the continuous structure of biofilm start to grow either in the filler or in the mushroom style depending on the location of the growth process. As biofilms develop, mature and enter the advanced stages, the EPS material increases around the bio-bacteria cells. The EPS distribution depends on where it is positioned in the rock system. If the bio-material is

localized only in the matrix, where there is no space, EPS will start to accumulate and build up layer upon layer in the same place. This biofilm formation style is described as filler growth. The texture of this biofilms is considered to be very thick which means that the bio-tubes will be closed and thus biofilm permeability ($K_{biofilm}$) decreases. In the case where bio-material will grow in pore space, the EPS substance has more space to grow and forms mushroom shape biofilms. This discontinuous mushroom shape biofilm will probably be more prone to getting disconnected upon decay and clogging the pore throats and in turn, reducing the porosity of the system.

The mushroom growth style appears to be dependent on the porosity of the system. The saturation models indicate that the mushroom growth style covered a larger volume than the filler model. This might be related to the fact that almost 80% of the increases in attenuation were reported by Davis *et al*. (2010) compared to only 45% decreases in attenuation observed. Moreover, since both experiments conducted by Davis *et al*. (2010) and Kwon and Ajo-Franklin ., (2012) did have an approximate porosity of 35%, this might be the reasoned that both studies reported a value of ~80% increase in attenuation. Therefore, probably the porosity acted as a threshold point in both experiments. In addition, at low biofilmsaturation, attenuation appears to be saturation proportional, i.e., as biofilmsaturation increases (effective porosity decreases), attenuation increases. For example, as an extreme case, 80% biofilmsaturation leads to ~80% decrease in amplitudes. At low biofilmsaturation (10-20%), however, the attenuation is inversely proportional to saturation. Although this appears to be counter-intuitive, we propose that at low bio-flim saturation, focused fluid flow can be achieved through formation of bio-tubes (interconnected and porous biofilmmembrane).

4.5 Model Limitations and Future Studies

The assumptions in rock physics models need to be carefully understood. For example, applying Gassmann's (1951) relations on high frequency data have revealed large disturbances between the models synthetic data and the observed real data (Dewar *et al*., 2001). However, in this work the Gassmann (1951) equation was used to represent ultrasonic data even though these relations are strictly valid only for low frequencies. The reason behind this is that Gassmann's (1951) fluid substitution relations are expected to work well at seismic frequencies significantly lower than f_{squirt}:

$$f\ squirt = \frac{K_{mineral}\,\alpha^3}{\mu} \tag{25}$$

Where α is the crack aspect ratio and μ is the fluid viscosity and in this case experimental frequency range (1-1.6 MHz) were much less than f_{squirt} value. In the future, further work on testing the designed rock physics models with different ranges of ultrasonic data and high frequency sample is recommended. Moreover, when the biofilm growth classification map was designed by the change in velocity concept, the assumption was that if a spot showed a loadbearing growth style no mushroom model growth is considered at all at the same spot throughout the experiment. However, keeping in mind the heterogeneity of microbial element and the complexity of biofilm formation, the simultaneous growth of biofilm in both styles at in one zone should be considered.

CHAPTER V

CONCLUSION

The growth of the biofilm associated in sediments poses large variability in the spatial and temporal properties of the sediment. However, so far little effort has been made to isolate changes caused by biofilm formation underground. Quantifying the time scales over which these vicissitudes take place due to biofilm growth is important for developing suitable experimental designs and for understanding how biofilms mediate sediment properties and processes. This paper describes rock physics models that were developed to explain seismic time-lapse velocity and attenuation data as function of biofilm saturation from the Davis *et al*. (2010) experiment. Heterogeneity in the structure of biofilm growth is the main cause of variability in the seismic acoustic data. Velocity alteration observed due to biofilm formation showed two dominate trends of continually increasing and continually decrease. To explain the velocity attributes, we used rock physics to replicate time-lapse velocity data from the Davis *et al.* (2010) experiment. Thus, we formulate the two models with appropriate time-lapse saturation of bio-films. Results presented that two separate biofilm growth phases are required based on biofilm saturation amount which influence biofilm saturation.

First, the low saturation phase which is the base stage in which biofilms coat the mineral grains in thin layer. Second, the high saturation phase or the surface phase that is also divided into two other growth styles based on biofilm formation location. The filler stage, at biofilms growth that occur within the sediment matrix. This growth style bears the load; biofilms increase bulk and shear strength and decrease density of the sediment system. The other biofilm growth style happens in pore space and form in a mushroom shape thus we called it Mushroom mode. In this mushroom mode growth style, biofilms decrease the density only without affecting the moduli. Increasing biofilm saturation in the filler style increases V_P while increasing biofilm saturation in the mushroom style decreases V_P.. Both growth styles create permeability changes in the system. In the early stages of biofilm development, permeability increases most likely due to formation of channels and bio-tubes. The base layer with low biofilm density acts as a bridge that connects pores together to open new channels around the matrix. However, no long and the permeability will suddenly decreases as biofilm continue to grow and biofilm saturation increase. This because the thicker the bio-material start to be, the more these channels start lose their transparency and transmission property.

Moreover, the results showed that biofilmsaturation will increases with time to a threshold value in which it stay almost constant over the period of observation. The thresholds depend on many factors that can control it such as clay content, grain size and porosity. Independently, we model attenuation as a function of porosity, permeability, and grain size. Attenuation behavior will act depending on biofilm saturation as well. That mean at high biofilmsaturation, attenuation appears to be saturation proportional, i.e., as biofilmsaturation increases (effective porosity decreases), attenuation increases.

To illustrate, as an extreme case, 80% biofilmsaturation leads to ~80% decrease in amplitudes. On the opposite side, at low biofilmsaturation (<10%), the attenuation is inversely proportional to saturation. The only way to explain the decrease in attenuation at low biofilm saturation is by increasing permeability. Although this appears to be counter-intuitive, we propose that at low biofilm saturation, focused fluid flow can be achieved through formation of bio-tubes (interconnected and porous biofilmmembrane). Our results suggest that rock physics model can serve as a quantitative tool for diagnosing physical property of bio-saturated sediments in in-situ conditions. More work, both experimental and numerical, is needed for confirmation.

REFERENCES

Aal, G. Z. A., Atekwana, E. A., and Atekwana, E. A., 2010, Effect of bioclogging in porous media on complex conductivity signatures: Journal of Geophysical Research-Biogeosciences, v. 115.

Aal, G. Z. A., Atekwana, E. A., Slater, L. D., and Atekwana, E. A., 2004, Effects of microbial processes on electrolytic and interfacial electrical properties of unconsolidated sediments: Geophysical Research Letters, v. 31, no. 12.

Adam, L., Batzle, M., Lewallen, K. T., and van Wijk, K., 2009, Seismic wave attenuation in carbonates: Journal of Geophysical Research-Solid Earth, v. 114.

Aggarwal, S., and Hozalski, R. M., 2010, Determination of biofilm mechanical properties from tensile tests performed using a micro-cantilever method: Biofouling, v. 26, no. 4, p. 479-486.

Allen, J. P., Atekwana, E. A., Atekwana, E. A., Duris, J. W., Werkema, D. D., and Rossbach, S., 2007, The microbial community structure in petroleum-contaminated sediments corresponds to geophysical signatures: Applied and Environmental Microbiology, v. 73, no. 9, p. 2860-2870.

Astley, O. M., Chanliaud, E., Donald, A. M., and Gidley, M. J., 2003, Tensile deformation of bacterial cellulose composites: International Journal of Biological Macromolecules, v. 32, no. 1-2, p. 28-35.

Atekwana, E. A., Atekwana, E., Legall, F. D., and Krishnamurthy, R. V., 2004, Field evidence for geophysical detection of subsurface zones of enhanced microbial activity: Geophysical Research Letters, v. 31, no. 23.

Atekwana, E. A., E. A. Atekwana, and D. D. Werkema (2006), Biogeophysics: The effects of microbial processes on geophysical properties of the shallow subsurface, in Applied Hydrogeophysics, NATO Sci. Ser., vol. 4, edited by H. Vereecken et al., pp. 161–193, Springer, New York.

Atekwana, E. A., and Slater, L. D., 2009, Biogeophysics: A New Frontier in Earth Science Research: Reviews of Geophysics, v. 47.

Babaia. F, a. C. F., 2000, VSP Interpretation, Estimation of Atteuation and Anisotropy: the National Enterprise of Geophysics (ENAGEO).

Batzle, M., and Wang, Z. J., 1992, Seismic Properties of Pore Fluids: Geophysics, v. 57, no. 11, p. 1396-1408.

Baveye, P., P. Vandevivere, B. L. Hoyle, P. C. DeLeo, and D. Sanchez de Lozada (1998), Environmental impact and mechanisms of the biological clogging of saturated soils and aquifer materials, Crit. Rev. Environ. Sci. Technol., 28(2), 123–191, doi:10.1080/10643389891254197.

Bendaoud, M., Vinogradov, E., Balashova, N. V., Kadouri, D. E., Kachlany, S. C., and Kaplan, J. B., 2011, Broad-Spectrum Biofilm Inhibition by Kingella kingae Exopolysaccharide: Journal of Bacteriology, v. 193, no. 15, p. 3879-3886.

Berryman, J. G., and Blair, S. C., 1987, Kozeny-Carman Relations and Image-Processing Methods for Estimating Darcy Constant: Journal of Applied Physics, v. 62, no. 6, p. 2221-2228.

Beyenal, H., Lewandowski, Z., and Harkin, G., 2004, Quantifying biofilm structure: Facts and fiction: Biofouling, v. 20, no. 1, p. 1-23.

Boadu, F. K., 1997, Rock properties and seismic attenuation: Neural network analysis: Pure and Applied Geophysics, v. 149, no. 3, p. 507-524.

Bouwer, E. J., H. H. M. Rijnaarts, A. B. Cunningham, and R. Gerlach (2000), Biofilms in porous media, in Biofilms II: Process Analysis and Applications, edited by J. D. Bryers, pp. 123–158, Wiley-Liss, Wilmington, Del.

Brinkman, H. C. (1949), A calculation of the viscous force exerted by a flowing fluid on a dense swarm of particles, Applied Scientific Research 1: 27–34.

Brovelli, A., F. Malaguerra, and D. A. Barry (2008), Bioclogging in porous media: Model development and sensitivity to initial conditions, Environ. Model. Softw., 24, 611–626.

Carcione, J. M., and Picotti, S., 2006, P-wave seismic attenuation by slow-wave diffusion: Effects of inhomogeneous rock properties: Geophysics, v. 71, no. 3, p. O1-O8.

Chellam, S. W., M. and Dawson,C. , 1992, Slip at a uniformly porous boundary: effect on fluid flow and mass transfer: Engineering Mathematics.

Costerton JW (2008) The evolution of the biofilm concept: a long and winding road. Sartoniana 21:59-67

Dai, J., et al., 2004. Detection and estimation of gas hydrates using rock physics and seismic inversion. The Leading Edge.

Davis, C. A., Atekwana, E., Atekwana, E., Slater, L. D., Rossbach, S., and Mormile, M. R., 2006, Microbial growth and biofilm formation in geologic media is detected with complex conductivity measurements: Geophysical Research Letters, v. 33, no. 18.

Davis, C. A., Pyrak-Nolte, L. J., Atekwana, E. A., Werkema, D. D., and Haugen, M. E., 2009, Microbial-induced heterogeneity in the acoustic properties of porous media: Geophysical Research Letters, 36, L21405, doi:10.1029/2009GL039569.

Davis, C. A., Pyrak-Nolte, L. J., Atekwana, E. A., Werkema, D. D., and Haugen, M. E., 2010, Acoustic and electrical property changes due to microbial growth and biofilm formation in porous media: Journal of Geophysical Research-Biogeosciences, v. 115.

DeJong, J. T., M. B. Fritzges, and K. Nusslein (2006), Microbially induced cementation to control sand response to undrained shear, J. Geotech. Geoenviron. Eng., 132(11), 1381–1392, doi:10.1061/(ASCE)1090-0241 (2006)132:11(1381).

DeJong, J. T., Mortensen, B. M., Martinez, B. C., and Nelson, D. C., 2010, Bio-mediated soil improvement: Ecological Engineering, v. 36, no. 2, p. 197-210.

Dunsmore, B. C., Jacobsen, A., Hall-Stoodley, L., Bass, C. J., Lappin-Scott, H. M., and Stoodley, P., 2002, The influence of fluid shear on the structure and material properties of sulphate-reducing bacterial biofilms: Journal of Industrial Microbiology & Biotechnology, v. 29, no. 6, p. 347-353.

Dunsmore, B. C., C. J. Bass, and H. M. Lappin-Scott (2004), A novel approach to investigate biofilm accumulation and bacterial transport in porous matrices, Environ. Microbiol., 6(2), 183–187, doi:10.1046/ j.1462-2920.2003.00546.x.

Dvorkin, J., and Nur, A., 1996, Elasticity of high-porosity sandstones: Theory for two North Sea data sets: Geophysics, v. 61, no. 5, p. 1363-1370.

Dvorkin, J., Nur, A., Uden, R., and Taner, T., Rock physics of gas hydrate reservoir, The Leading Edge, 22, 842-847, 2003.

Dvorkin, J., and Uden, R., Seismic wave attenuation in a methane hydrate reservoir, The LeadingEdge, 23, 8, 2004.

Ehrlich, H. L., 1997, Microbes and metals: Applied Microbiology and Biotechnology, v. 48, no. 6, p. 687-692.

Ehrlich, H.L., 1998, Geomicrobiology: its significance for geology: Earth-Science Reviews, v. 45, no. 1-2, p. 45-60.

Gassmann, F., 1951, Elastic Waves Through a Packing of Spheres Geophysics, v. 16, no. 4.

Guhados, G., Wan, W. K., and Hutter, J. L., 2005, Measurement of the elastic modulus of single bacterial cellulose fibers using atomic force microscopy: Langmuir, v. 21, no. 14, p. 6642-6646.

Gurevich, B., and Ciz, R., 2006, Shear wave dispersion and attenuation in periodic systems of alternating solid and viscous fluid layers: International Journal of Solids and Structures, v. 43, no. 25-26, p. 7673-7683.

Gurevich, B., Makarynska, D., de Paula, O. B., and Pervukhina, M., 2010, A simple model for squirt-flow dispersion and attenuation in fluid-saturated granular rocks: Geophysics, v. 75, no. 6, p. N109-N120.

Gurevich, B., Zyrianov, V. B., and Lopatnikov, S. L., 1997, Seismic attenuation in finely layered porous rocks: Effects of fluid flow and scattering: Geophysics, v. 62, no. 1, p. 319-324.

Han, D., and Batzle, M.(2004).Gassmann's equation and fluid-saturation effects on seismic velocities. GEOPHYSICS, VOL. 69, NO. 2 (MARCH-APRIL 2004); P. 398–405, 8 FIGS., 2 TABLES.10.1190/1.1707059

Hedlin, K. M., L. & Margrave, G., 2004, Seismic Attenuation Problem: Annual International Meeting, Society of Exploration Geophysicists,.

Hiebert, F. K., and Bennett, P. C., 1992, Microbial Control of Silicate Weathering in Organic-Rich Ground-Water: Science, v. 258, no. 5080, p. 278-281.

Hill, R., 1952, The Elastic Behaviour of a Crystalline Aggregate: Proceedings of the Physical Society. Section A, v. 65, no. 5.

Horn, H., Wasche, S., and Hempel, D. C., 2002, Simulation of biofilm growth, substrate conversion and mass transfer under different hydrodynamic conditions: Water Science and Technology, v. 46, no. 1-2, p. 249-252.

Hsieh, Y.-C. Y., H. Nogi, M.Eichhorn, S. J., 2008, An estimation of the Young's modulus of bacterial cellulose filaments: Springer Science+Business Media.

Hubbard, S.S., K. Williams, M. Conrad, B. Faybishenko, J. Peterson, J. Chen, P. Long and T. Hazen, Geophysical monitoring of hydrological and biogeochemical transformations associated with Cr(VI) Biostimulation, Environmental Science and Technology, DOI 10.1021/es071702s,2008

Karatas, I.(2008).Microbiological Improvement of the Physical Properties of Soils.

Klapper, I., Rupp, C. J., Cargo, R., Purvedorj, B., and Stoodley, P., 2002, Viscoelastic fluid description of bacterial biofilm material properties: Biotechnology and Bioengineering, v. 80, no. 3, p. 289-296.

Konhauser, K. O., and Gingras, M. K., 2007, Linking geomicrobiology with ichnology in marine sediments: Palaios, v. 22, no. 4, p. 339-342.

Kwon, T.-H. A.-F., Jonathan; Lawrence Berkeley 2012, Seismic Responses during Permeability Reduction due to Biopolymer Clogging in Unconsolidated Porous Media: Geophysics.

Johnston-C-A, Pinay-G, Arens-C, Naiman-R-J., (1995). Influence of soil properties on the biogeochemistry of a beaver meadow hydrosequence. Soil-Science-Society-of-America-Journal; 59 (6) 1789-1799.

Lappan, R. E., and Fogler, H. S., 1996, Reduction of porous media permeability from in situ Leuconostoc mesenteroides growth and dextran production: Biotechnology and Bioengineering, 50, 6-15.

Laspidou, C., and Aravas, N., 2007, Variation in the mechanical properties of a porous multi-phase biofilm under compression due to void closure: Water Science and Technology, v. 55, no. 8-9, p. 447-453.

Le Chatelier, H. a. B. O., 1898, Limits of Flammability of Gaseous Mixtures: Bulletin de la Société Chimique de France v. 19, p. 483–488.

Li, X., Zhong, L. R., and Pyrak-Nolte, L. J., 2001, Physics of partially saturated porous media: Residual saturation and seismic-wave propagation: Annual Review of Earth and Planetary Sciences, v. 29, p. 419-460.

Marshall, K. C. (1992), Biofilms: An overview of bacterial adhesion, activity, and control at surfaces, ASM News, 58(4), 202–207.

Masson, Y. J., and Pride, S. R., 2011, Seismic attenuation due to patchy saturation: Journal of Geophysical Research-Solid Earth, v. 116.

Maultzsch, S., Chapman, M., Liu, E., and Li, X. Y., 2007, Modelling and analysis of attenuation anisotropy in multi-azimuth VSP data from the Clair field: Geophysical Prospecting, v. 55, no. 5, p. 627-642.

Mavko, G., Kjartansson, E., and Winkler, K., 1979, Seismic-Wave Attenuation in Rocks: Reviews of Geophysics, v. 17, no. 6, p. 1155-1164.

Miqueleto, A. P., Dolosic, C. C., Pozzi, E., Foresti, E., and Zaiat, M., 2010, Influence of carbon sources and C/N ratio on (EPS) production in anaerobic sequencing batch biofilm reactors for wastewater treatment: Bioresource Technology, v. 101, no. 4, p. 1324-1330.

Muller, T. M., Gurevich, B., and Lebedev, M., 2010, Seismic wave attenuation and dispersion resulting from wave-induced flow in porous rocks - A review: Geophysics, v. 75, no. 5, p. A147-A164.

Murphy, W. F., Winkler, K. W., and Kleinberg, R. L., 1986, Acoustic Relaxation in Sedimentary-Rocks - Dependence on Grain Contacts and Fluid Saturation: Geophysics, v. 51, no. 3, p. 757-766.

Nishi, Y., Uryu, M., Yamanaka, S., Watanabe, K., Kitamura, N., Iguchi, M., and Mitsuhashi, S., 1990, The Structure and Mechanical-Properties of Sheets Prepared from Bacterial Cellulose .2. Improvement of the Mechanical-Properties of Sheets and Their Applicability to Diaphragms of Electroacoustic Transducers: Journal of Materials Science, v. 25, no. 6, p. 2997-3001.

Ntarlagiannis, D., K. H. Williams, L. D. Slater, and S. S. Hubbard, 2005a, Low frequency electrical response to microbial induced sulfide precipitation: JGR, G02009

Ntarlagiannis, D., N. Yee, and L. Slater, 2005b, On the low-frequency electrical polarization of bacterial cells in sands: Geophys. Res. Lett. , 32(doi:10.1029/2005GL024751),L24402.

Ntarlagiannis, D., E. A. Atekwana, E. A. Hill, and Y. Gorby, 2007, Microbial Nanowires

Picioreanu, C., Katuri, K. P., van Loosdrecht, M. C. M., Head, I. M., and Scott, K., 2010, Modelling microbial fuel cells with suspended cells and added electron transfer mediator: Journal of Applied Electrochemistry, v. 40, no. 1, p. 151-162.

Picioreanu, C., van Loosdrecht, M. C. M., and Heijnen, J. J., 1999, Discrete-differential modelling of biofilm structure: Water Science and Technology, v. 39, no. 7, p. 115-122.

Pintelon, T. R. R., Picioreanu, C., van Loosdrecht, M. C. M., and Johns, M. L., 2012, The effect of biofilm permeability on bioclogging of porous media: Biotechnology and Bioengineering, v. 109, no. 4, p. 1031-1042.

Roth, E. G., Wiens, D. A., and Zhao, D. P., 2000, An empirical relationship between seismic attenuation and velocity anomalies in the upper mantle: Geophysical Research Letters, v. 27, no. 5, p. 601-604.

Sakurada, I., Nukushina, Y., and Ito, T., 1962, Experimental Determination of Elastic Modulus of Crystalline Regions in Oriented Polymers: Journal of Polymer Science, v. 57, no. 165, p. 651-&.

Shafahi, M., and Vafai, K., 2009, Biofilm affected characteristics of porous structures: International Journal of Heat and Mass Transfer, v. 52, no. 3-4, p. 574-581.

Shaw, T., Winston, M., Rupp, C. J., Klapper, I., and Stoodley, P., 2004, Commonality of elastic relaxation times in biofilms: Physical Review Letters, v. 93, no. 9.

Slater, L. D., and Lesmes, D., 2002, IP interpretation in environmental investigations: Geophysics, v. 67, no. 1, p. 77-88.

Slater, L., F. D. Day-Lewis, D. Ntarlagiannis, M. O'Brien, and N. Yee (2009), Geoelectrical measurement and modeling of biogeochemical breakthrough behavior during microbial activity, Geophys. Res. Lett., 36, L14402, doi:10.1029/2009GL038695.

Smith, F. L., and Harvey, A. H., 2007, Avoid common pitfalls when using Henry's law: Chemical Engineering Progress, v. 103, no. 9, p. 33-39.

Stoodley, P., Cargo, R., Rupp, C. J., Wilson, S., and Klapper, I., 2002, Biofilm material properties as related to shear-induced deformation and detachment phenomena: Journal of Industrial Microbiology & Biotechnology, v. 29, no. 6, p. 361-367.

Stoodley, P., Dodds, I., Boyle, J. D., and Lappin-Scott, H. M., 1999, Influence of hydrodynamics and nutrients on biofilm structure: Journal of Applied Microbiology, v. 85, p. 19s-28s.

Stoodley, P., Lewandowski, Z., Boyle, J. D., and Lappin-Scott, H. M., 1998, Oscillation characteristics of biofilm streamers in turbulent flowing water as related to drag and pressure drop: Biotechnology and Bioengineering, v. 57, no. 5, p. 536-544.

Takahashi,I. (2005).Quantifying Information and Uncertainty of rock Property Estimation from Seismic Data.

Tajima, K., Fujiwara, M., and Takai, M., 1995, Biological-Control of Cellulose: Macromolecular Symposia, v. 99, p. 149-155.

Taylor, S. W., and Jaffe, P. R., 1990, Biofilm Growth and the Related Changes in the Physical Properties of a Porous-Medium .1. Experimental Investigation: Water Resources Research, 26, 2153-2159.

Teng, L.(1998). Seismic And Rock-Physics Characterization of Fractured Reservoirs. A Dissertation Submitted to the Department of Geophysics and the Committee on Graduate Studies of Stanford University.

Towler, B. W., Cunningham, A., Stoodley, P., and McKittrick, L., 2007, A model of fluid-biofilm interaction using a Burger material law: Biotechnology and Bioengineering, v. 96, no. 2, p. 259-271.

Towler, B. W., Rupp, C. J., Cunningham, A. B., and Stoodley, P., 2003, Viscoelastic properties of a mixed culture biofilm from rheometer creep analysis: Biofouling, v. 19, no. 5, p. 279-285.

Valls, M., and de Lorenzo, V., 2002, Exploiting the genetic and biochemical capacities of bacteria for the remediation of heavy metal pollution: Fems Microbiology Reviews, v. 26, no. 4, p. 327-338.

Wang, Z., (2011). Fundamentals of Seismic Rock Physics. GEOPHYSICS, VOL. 66, NO. 2 (MARCH-APRIL 2001); P. 398–412.

Walsh, J. B., 1995, Seismic Attenuation in Partially Saturated Rock: Journal of Geophysical Research-Solid Earth, v. 100, no. B8, p. 15407-15424.

Watson, J. H. P., Ellwood, D. C., Deng, Q. X., Mikhalovsky, S., Hayter, C. E., and Evans, J., 1995, Heavy-Metal Adsorption on Bacterially Produced Fes: Minerals Engineering, v. 8, no. 10, p. 1097-1108.

West, O. R., Siegrist, R. L., Gierke, J. S., Schmunk, S. W., Lucero, A. J., and Jennings, H. L., 1995, In-Situ Mixed Region Vapor Stripping in Low-Permeability Media .1. Process Features and Laboratory Experiments: Environmental Science & Technology, v. 29, no. 9, p. 2191-2197.

Williams, K. H. (2002), Monitoring microbe-induced physical property changes using high-frequency acoustic waveform data: Toward the development of a microbial megascope, M.S. thesis, Univ. of Calif., Berkeley.

Williams, K. H., Ntarlagiannis, D., Slater, L. D., Dohnalkova, A., Hubbard, S. S., and Banfield, J. F., 2005, Geophysical imaging of stimulated microbial biomineralization: Environmental Science & Technology, v. 39, no. 19, p. 7592-7600.

Williams, K., Kemna, A., Wilkins, M.(2009). Geophysical Monitoring of Coupled Microbial and Geochemical Processes During Stimulated Subsurface Bioremediation. Environ. Sci. Technol., 43 (17), pp 6717–6723,DOI: 10.1021/es900855j.

Winkler, K., and Nur, A., 1980, The Relative Effects of Pore Fluids on Seismic Attenuation and Velocities: Geophysics, v. 45, no. 4, p. 534-534.

Winkler, K., Nur, A., and Gladwin, M., 1979, Friction and Seismic Attenuation in Rocks: Nature, v. 277, no. 5697, p. 528-531.

Winkler, K. W., and Nur, A., 1982, Seismic Attenuation - Effects of Pore Fluids and Frictional Sliding: Geophysics, v. 47, no. 1, p. 1-15.

Yamanaka, H., Shimatani, S., Tanaka, M., Katsu, T., Ono, B., and Shinoda, S., 1989, Susceptibility of Erythrocytes from Several Animal Species to Vibrio-Vulnificus Hemolysin: Fems Microbiology Letters, v. 61, no. 3, p. 251-256.

Yen, T. F. (1990). Microbial Enhanced Oil Recovery: Principle and Practice.Boca Raton, FL: CRC Press.

Zajic, J. E., Cooper, C. D., Jack, T. R., and Kosaroc, N. (1983). Microbial Enhanced Oil Recovery. Tulsa, OK: Penn Well Books.

Table 1.Elastic moduli and densities of Quartz and some fluid components.

Component	Bulk Modulus (GPa)	Shear Modulus (GPa)	Density (g/cc)
Quartz	36.60	45.00	2.650
water	2.330	0.00	1.029
Gas	0.017	0.00	0.112

Table 2. Mechanical Properties of Bacterial Cellulose

Biofilm Density (g/m^3)	Biofilm Tensile stress (GPa)	Young's moduli (GPa)	The bacteria moduli (GPa)	Biofilm Shear Stress (Pa)	Author
		15			Yamanaka et al. (1989)
		30			Nishi et al. (1990)
		30–40			Tajima et al. (1995)
0.11			0.13		Astley et al. (2003)
			20–21		Yano et al. (2005)
		64.6-99.6($x10^{-9}$)		0.005-5.1	Klapperet al. (2002)
		17- 240($x10^{-9}$)			Stoodley et al. (1999)
		6.5-0.5($x10^{-6}$)			Ko¨rstgens et al. (2001)
		63.9-283($x10^{-9}$)		0.05-55	Stoodley et al. (1998)
			114		Hsieh (2008)
0.027-0.115				1.12	Horn et al. (1995)
		$6x10^{-8}$			Stoodley et al. (2002)
			1.27+0.28($x10^{-6}$)		Towler et al.(2003)
0.09		78 +/- 17			Guhados et al. (2005)
					Sakurada et al. (1962)
	0.5-1($x10^{-6}$)	6-5($x10^{-6}$)		0.2 - 24	Aggrawal and Hozalaski(2010)

Table 3. log PCO_2 values which are obtained using the Phreeq-C geochemical software Henry's equation.

Alkalinity of water	Log(PCO2) at pH=7	Log(PCO2) at pH=5	Log(PCO2) at pH=4.5	Log(PCO2) at pH=4
50	-2.1983	0.11	0.316	0.8454
100	-1.905	0.4039	0.6068	1.1236
150	-1.7286	0.5757	0.7779	1.2912

Table 4. PCO_2 values in (mol/liter).

Alkalinity of water	pH=7	pH=5	pH=4.5	pH=4
50	0.0063	1.288	2.0711	7.005
100	0.01245	2.5345	4.0439	13.292
150	0.01868	3.7644	5.997	19.552

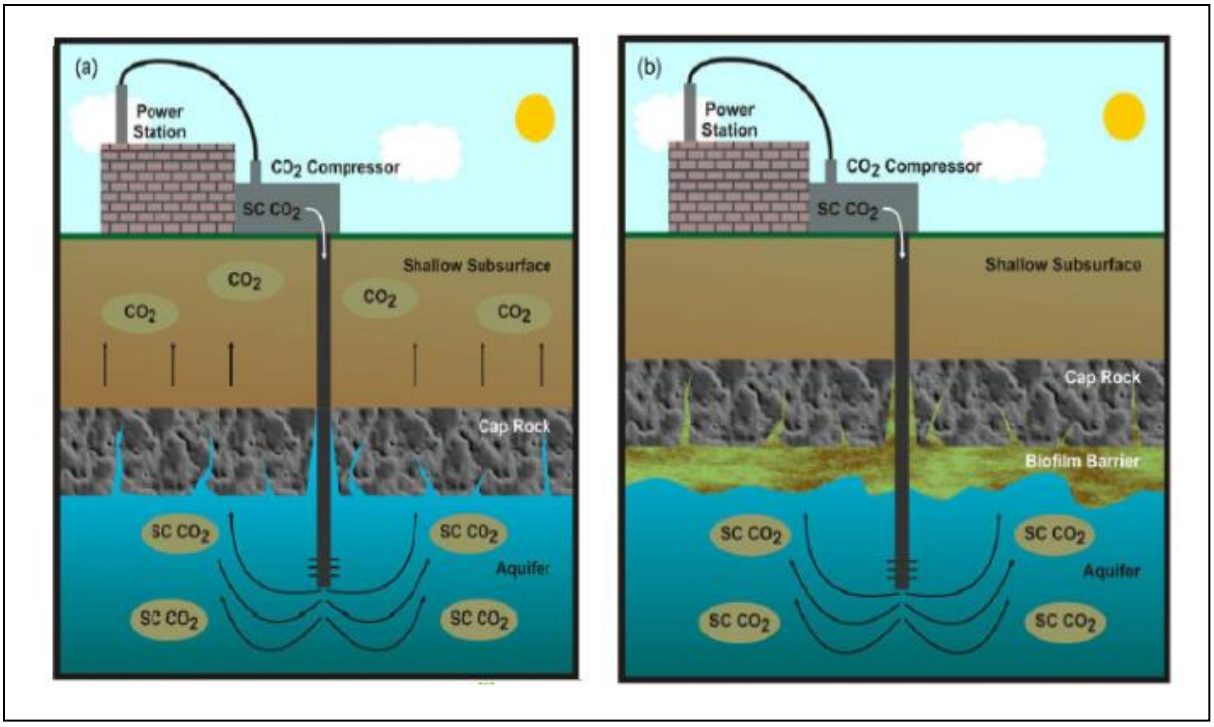

Figure 1.Conceptual illustration of supercritical CO_2 leakage mitigation using deep subsurface biofilm barriers (a) Potential upward leakage of CO_2 from deep subsurface (b) Reduced upward leakage of CO_2 due to engineered biofilm barrier (Mitchell et al. 2009).

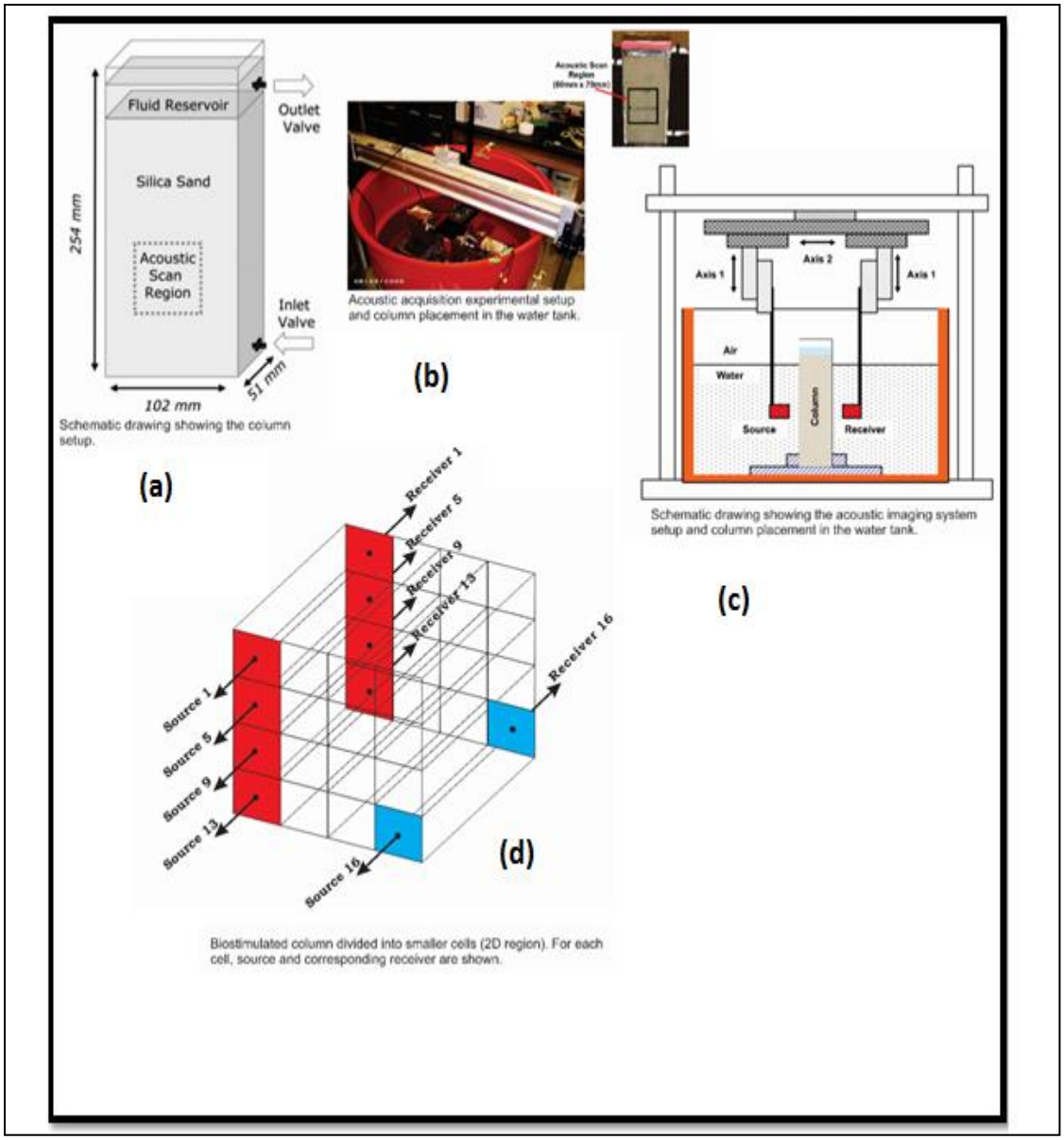

Figure 2. Experimental setup for the acoustic measurement used: (a)Schematic drawing showing the column setup, (b)Acoustic experimental setup and column placement in the water tank, (c) drawing showing the acoustic imaging system setup and (d) Biostimulated column divided into smaller (Davis et al., 2010).

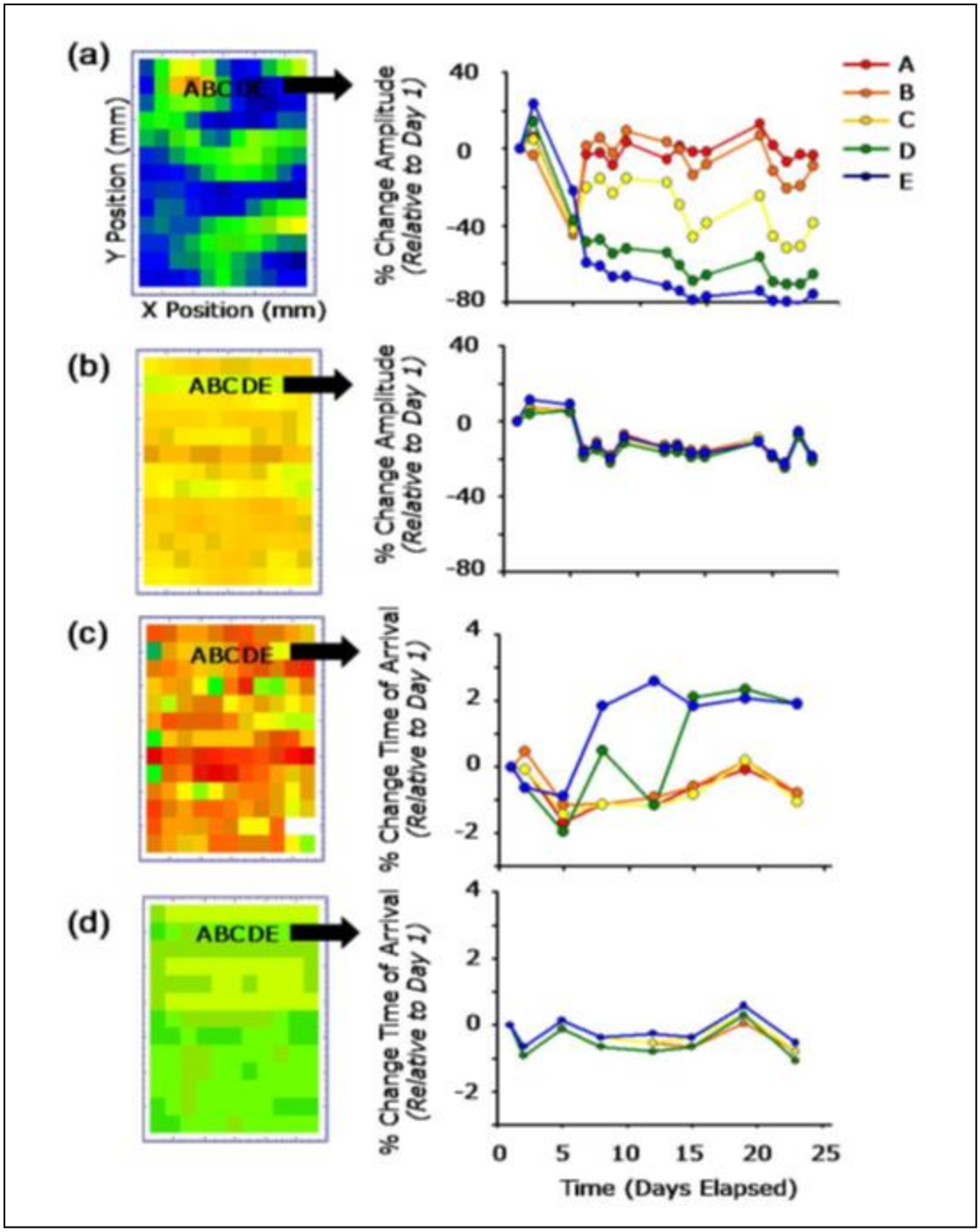

Figure 3.Two-dimensional amplitude scans obtained from day 29 for the (a) biostimulated and (b) control columns, with the select scan region (positions A–E) plotted temporally to the right. Similarly, the 2-D time of arrival scans obtained from day 29 for the (c) biostimulated and (d) control columns, with the select scan region (positions A–E) plotted to the right (Davis et al., 2010).

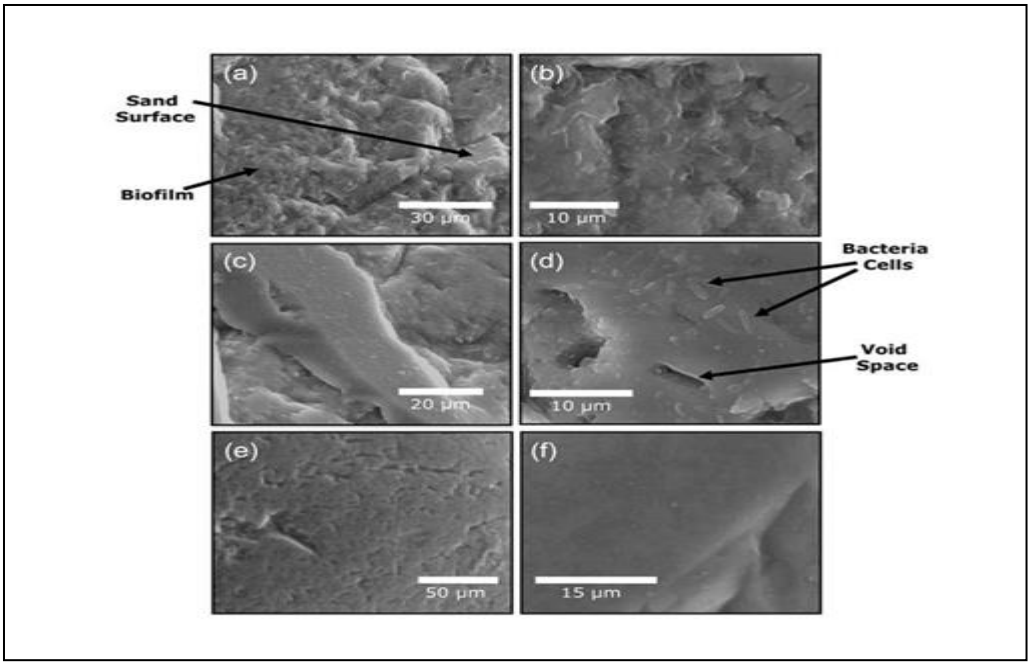

Figure 4.SEM images from sand samples: (a & b) patchy growth from the bio-stimulated column, and (c & d) non-patchy growth from the same column; (e & f) Images from the control column (Davis et al., 2010).

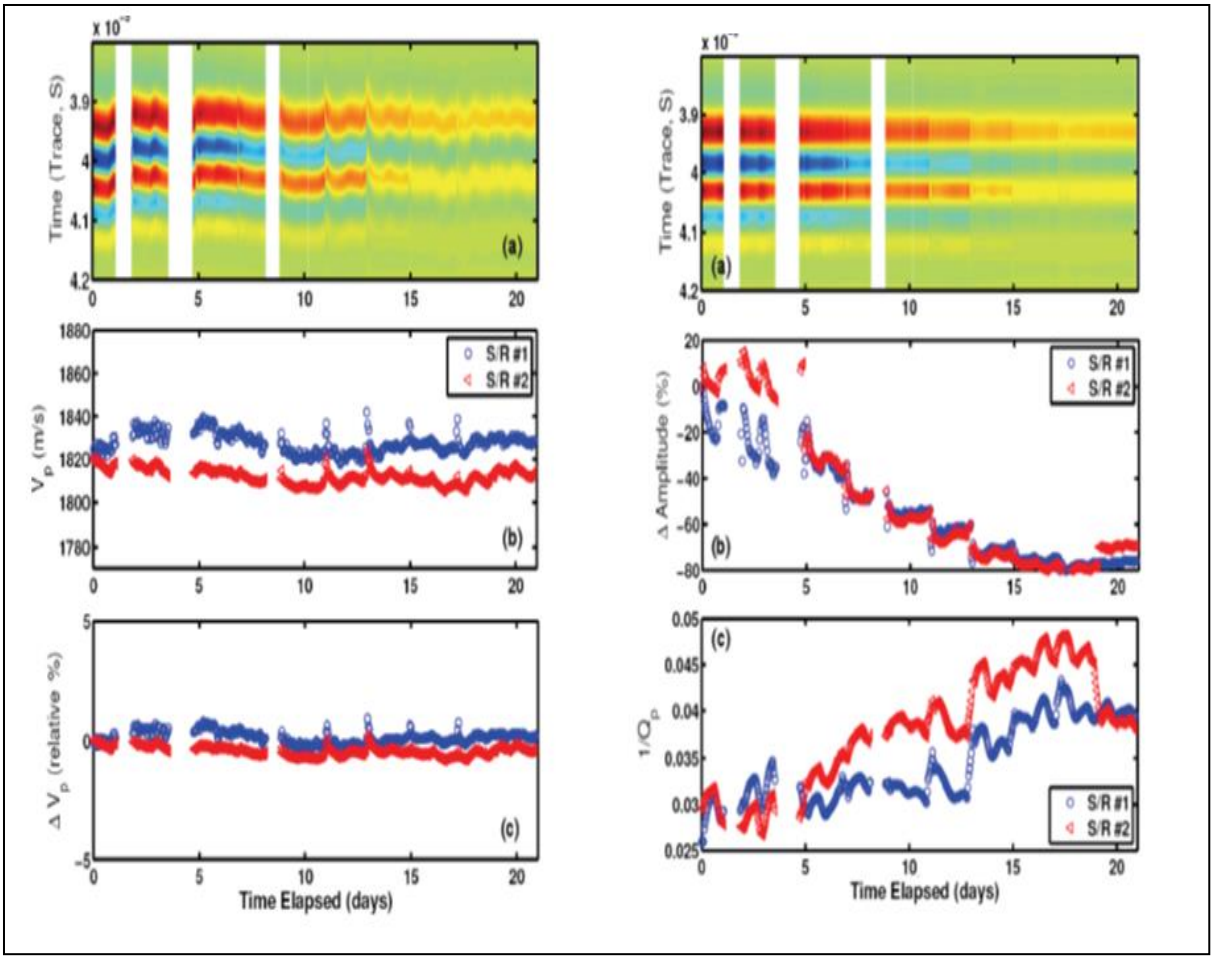

Figure 5. Left side: (a) P-wave signatures of biopolymer formation experiment 1, (b) P-wave velocity with time, (c) Relative P-wave velocity changes. Right side: (a) P-wave signatures experiment 2, (b) Relative amplitude changes to the initial amplitudes and (c) attenuation (1/QP) changes over a course of the first and second experiment (Kwon and Ajo-Franklin, 2011).

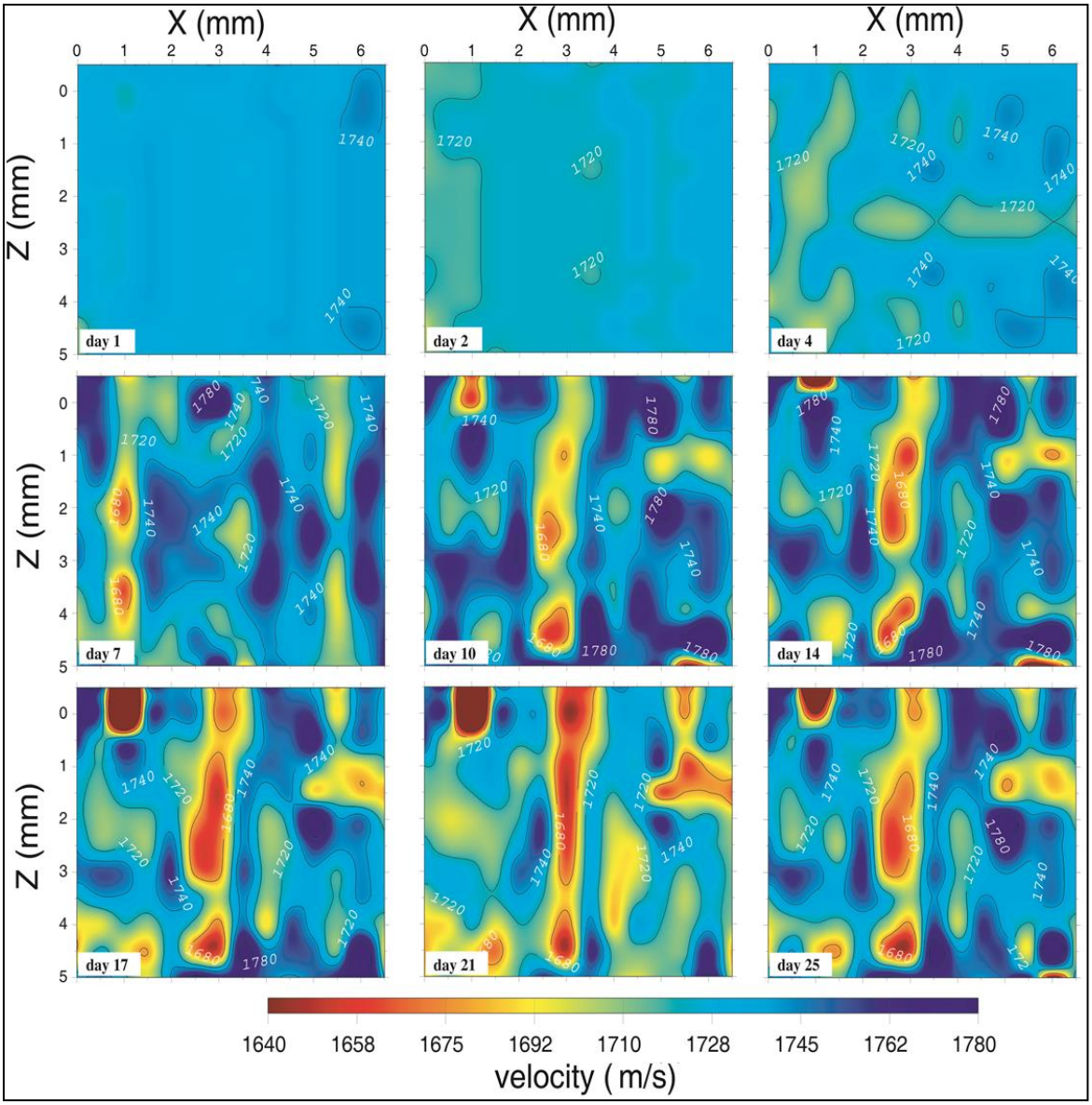

Figure 6.2D-biostimulated Velocity model from straight-ray tomography. The models show a fairly random distribution of high and low velocity patches in the first 7 days. From Day 10 onwards a vertical zone of low velocity starts appearing in the center. We speculate this zone to be weak and higher porosity which is more conducive to fluid flow. This gradual change in porosity could be as a result of preparation of the sample box or due to the growth of biofilms themselves.

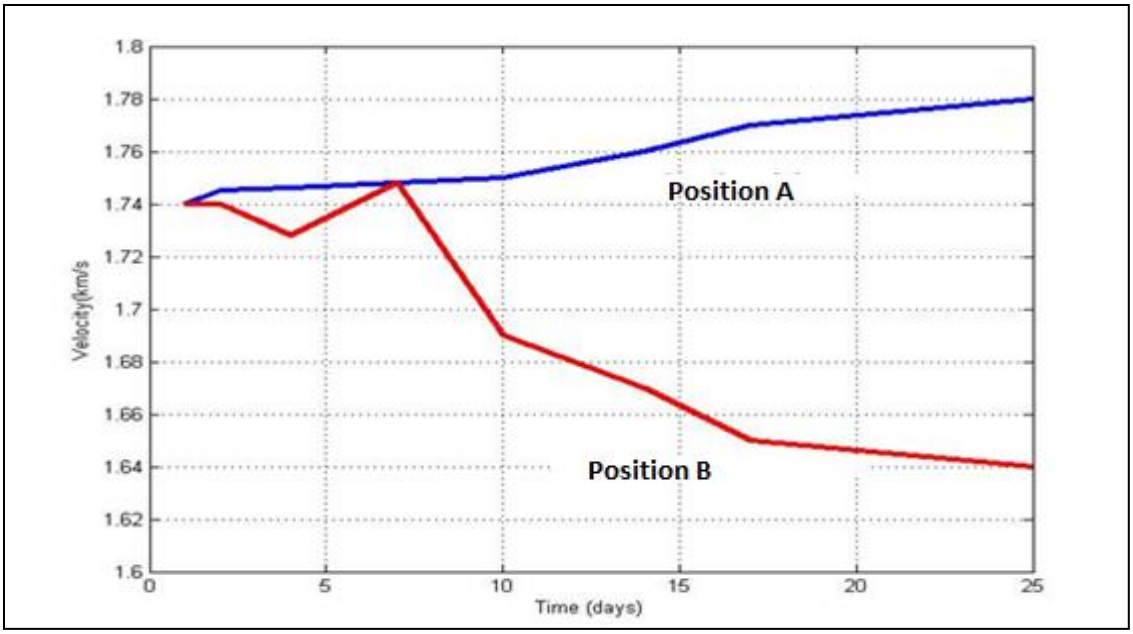

Figure 7.Temporal changes in velocities: (A) an increase in velocity with time, (B) Relative decrease in velocity.

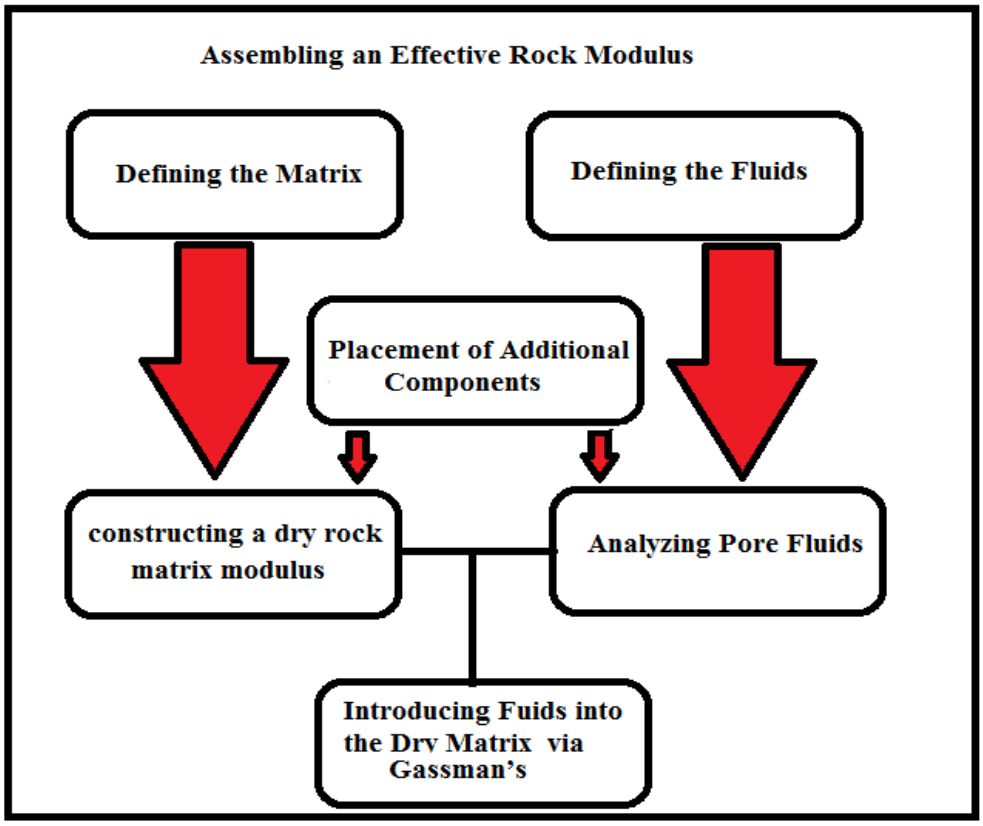

Figure 8. Rock phyiscs basic concept of constructing an effective rock modulus flow chart.

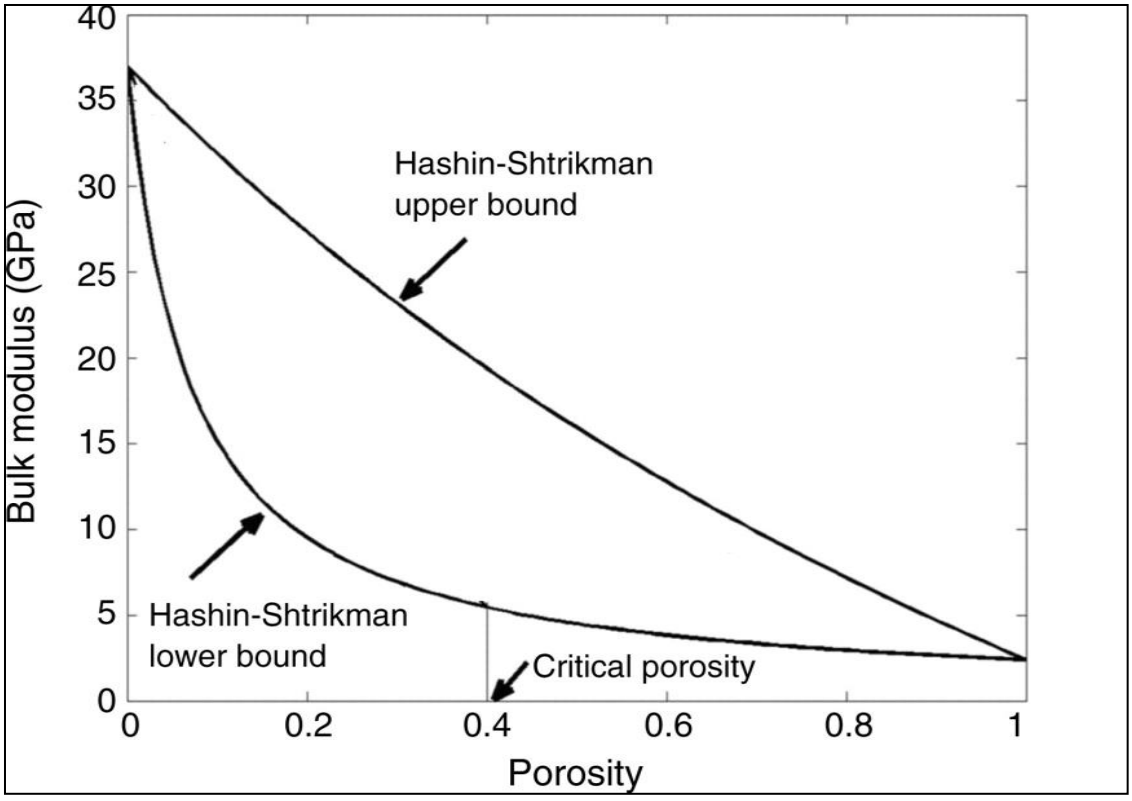

Figure 1.Hashin-Shtrikman bound that connect the two extreme end points at zero & critical porosity.

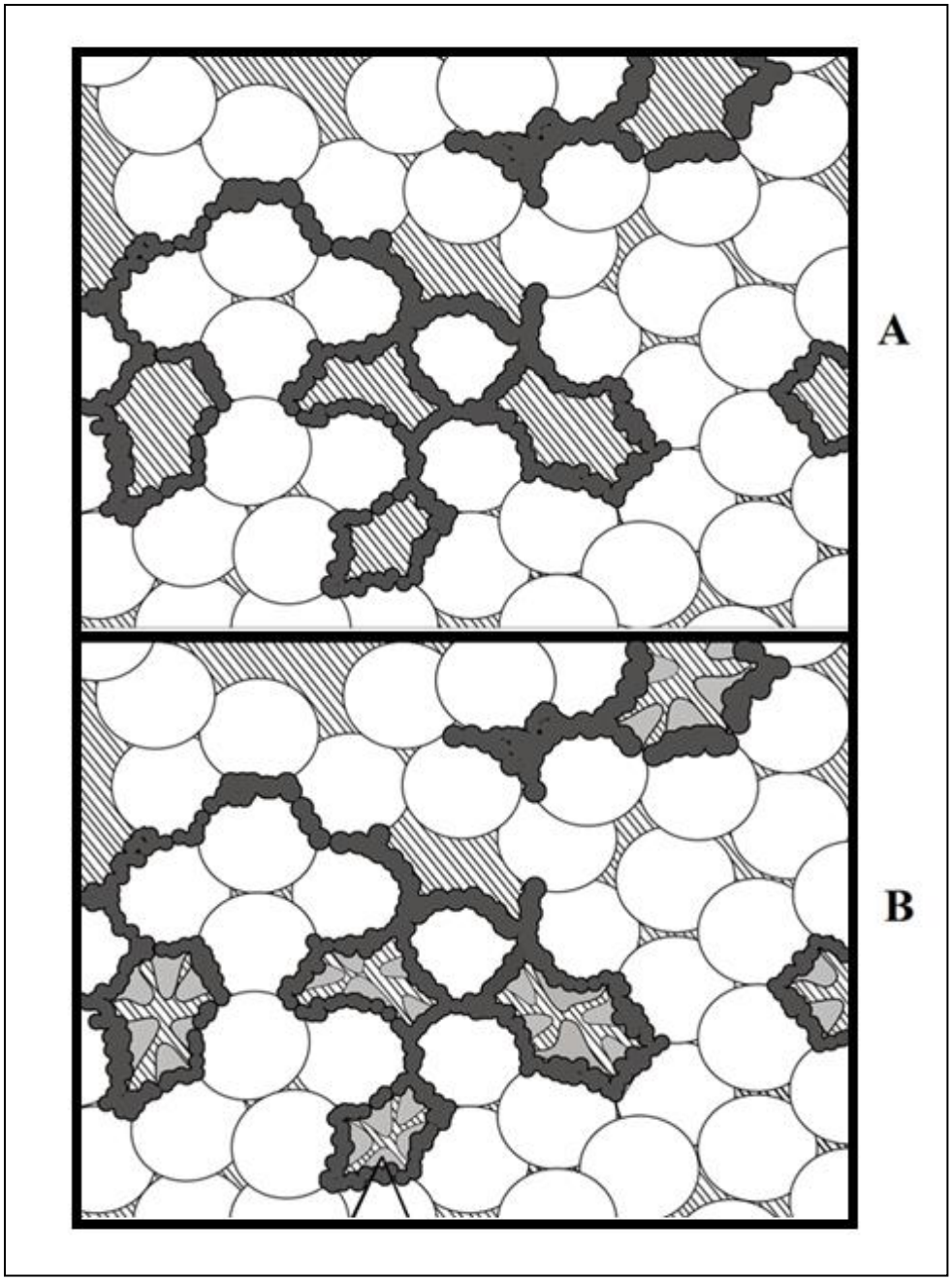

Figure 2.Microbial Growth and biofilm formation phases: (A) Base phase at which a thin layer of biofilm sheet start to expand and cover the grain and (B)surface phase where to different in-continuous bio-growth style occur .

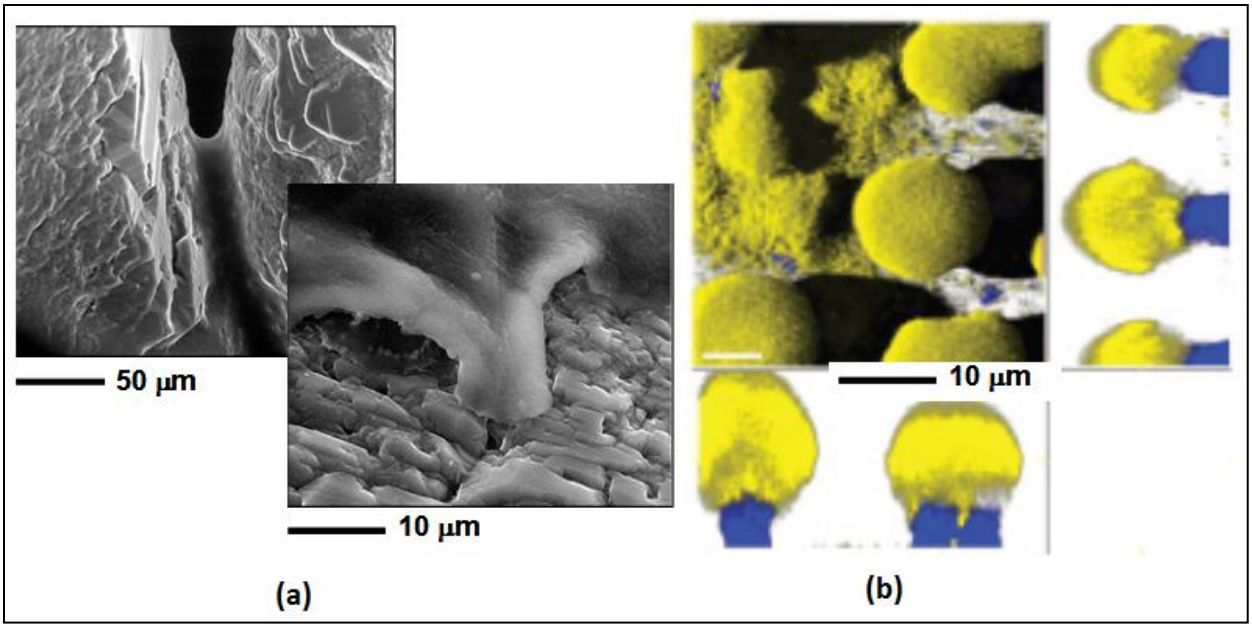

Figure 3.Surface phase biofilm growth styles: (a) Loadbearing and (b) mushroom mode.

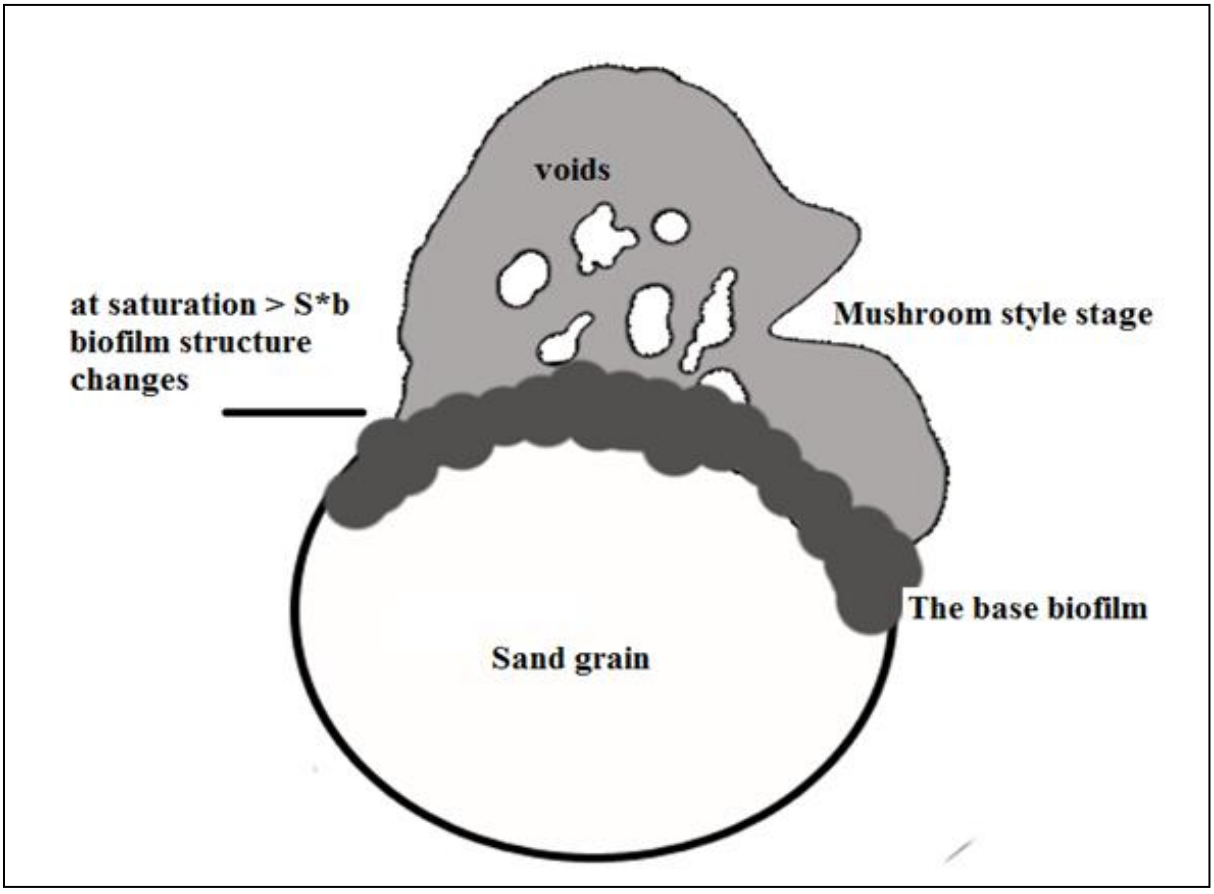

Figure 4. Mushroom growth style structure.

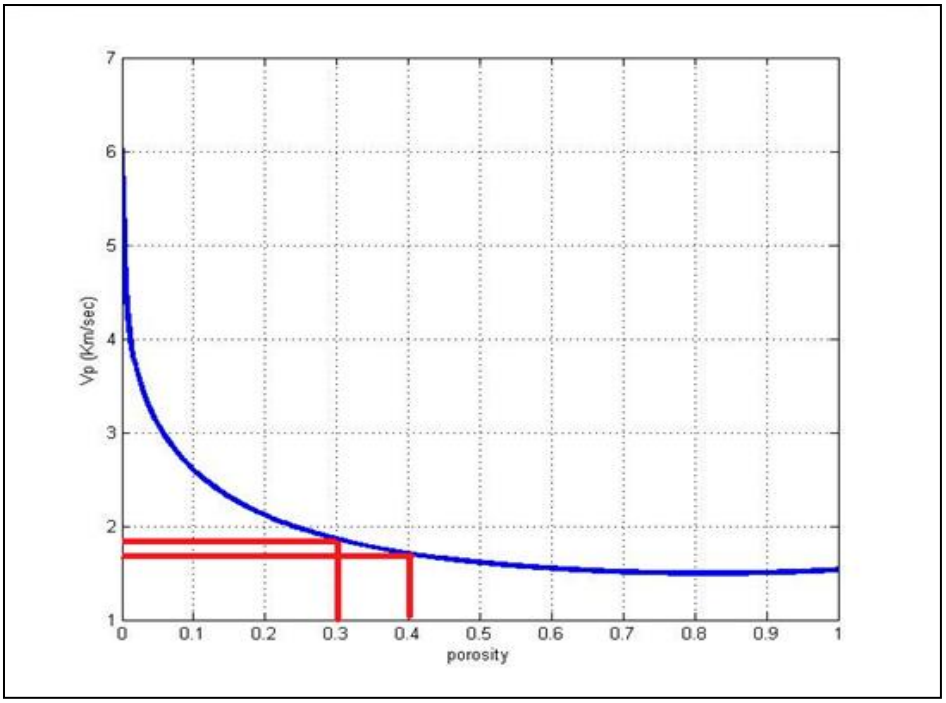

Figure 5.Schematic presenting velocity vs. porosity was done to investigate porosity of the control system.

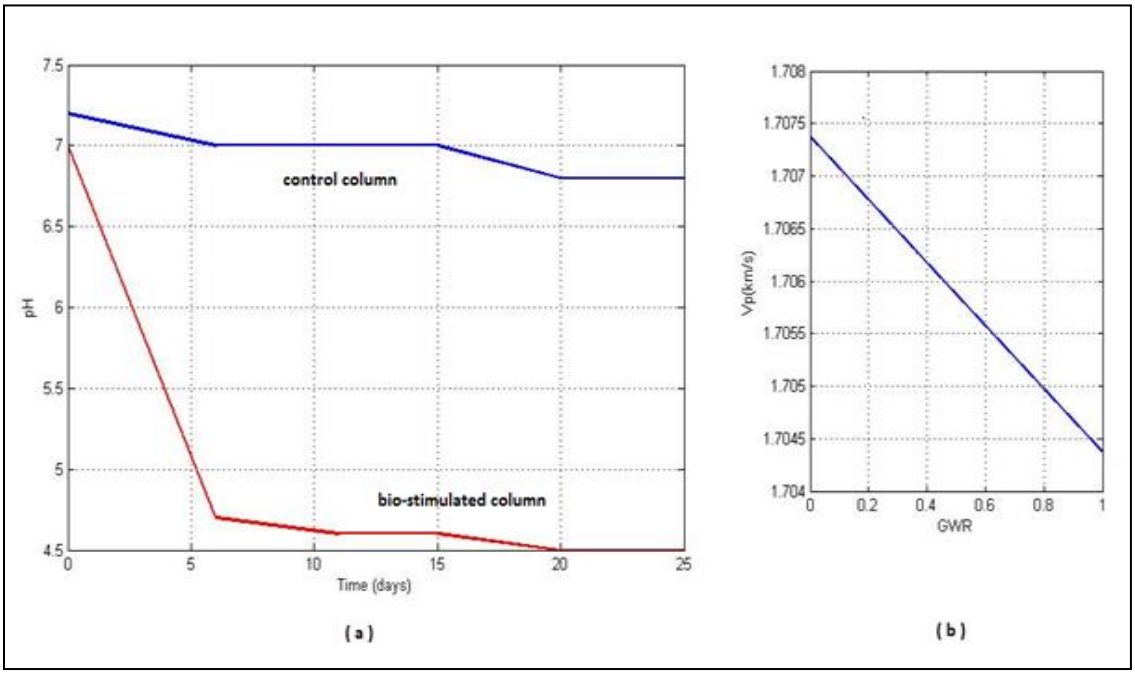

Figure 6. Plots showing the (a) pH results and (b) velocity change due to dissolved gas in water represented as increase in GWR.

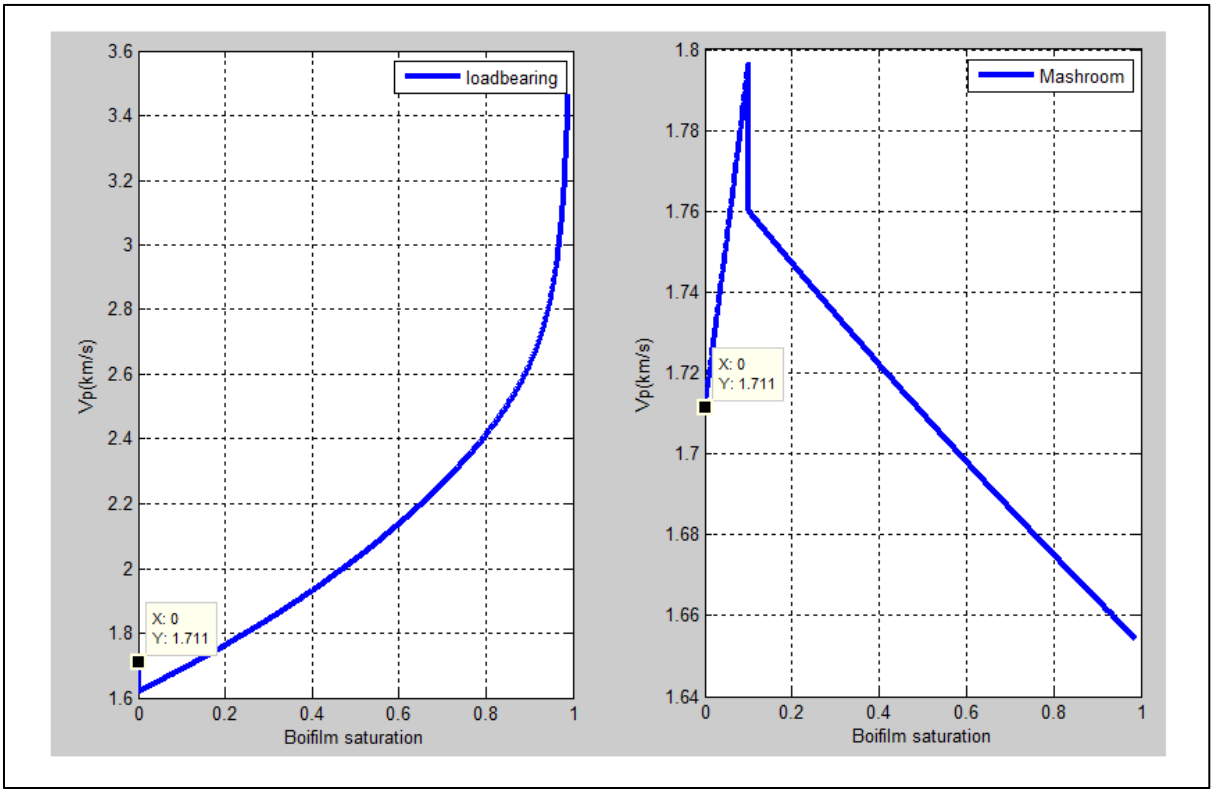

Figure 7.Synthetic data velocity variations with microbial growth in the system applying: (left) load bearing model; (right) Mushroom model.

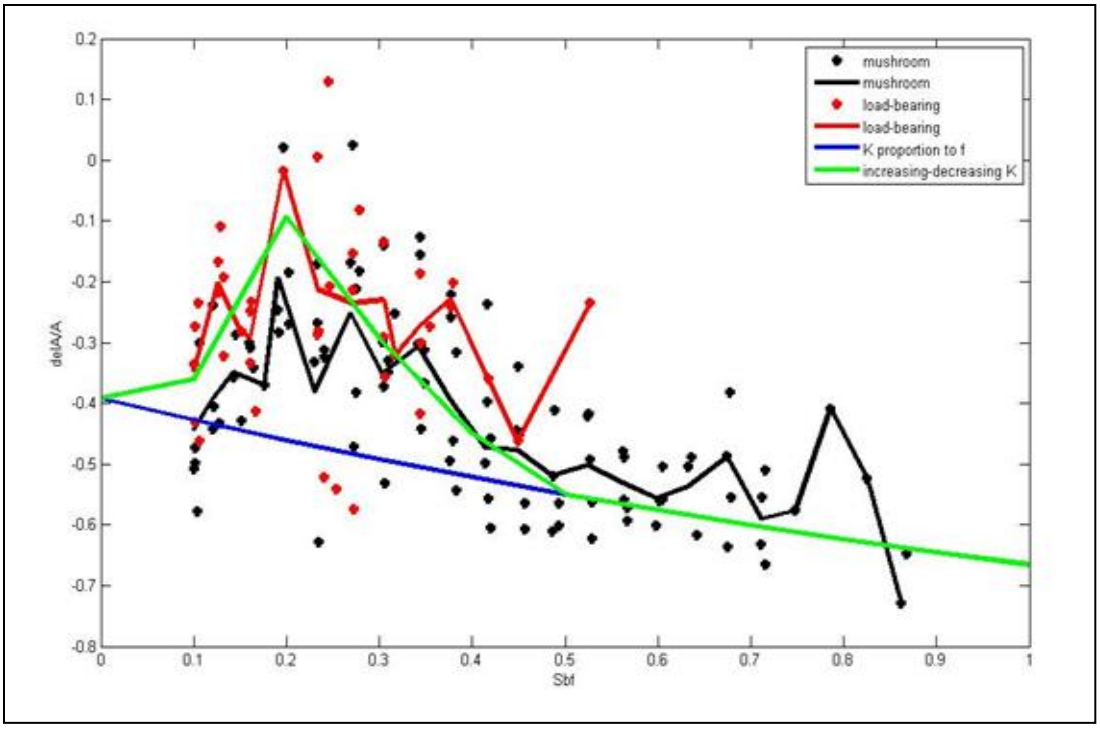

Figure 16.Attenuation models for the two biofilm growth styles and permeability changes (green) due to microbial growth.

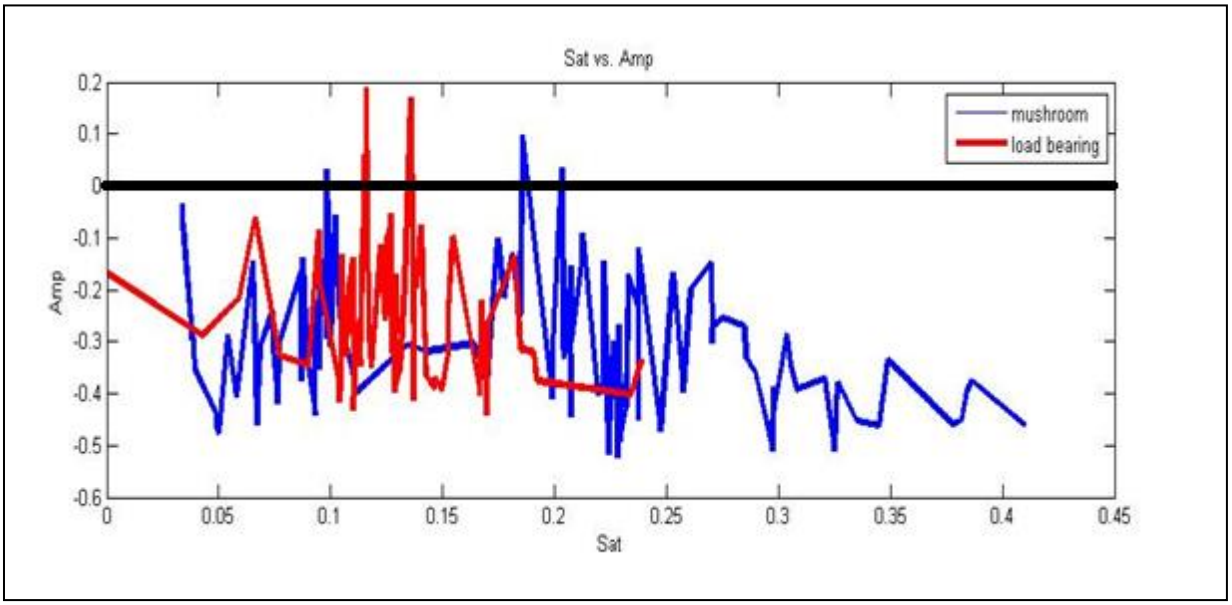

Figure 17.Amplitude alterations for the two different growth style: (red) loadbearing; (blue) mushroom with respect to biofilm saturation.

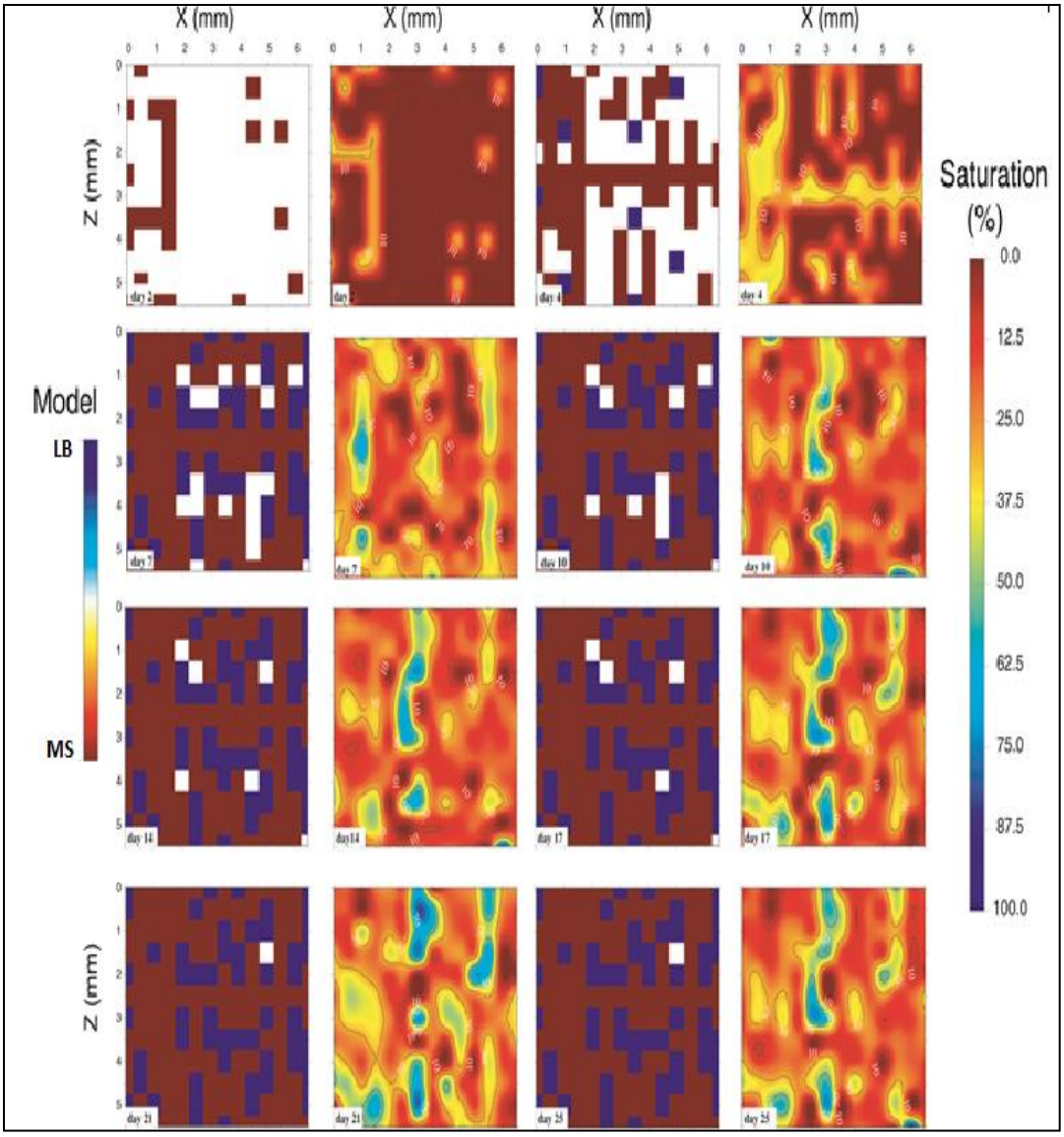

Figure 18.2-D maps of the biofilm growth type Classification and biofilm Saturation distributions where LB: Loadbearing mode and MS: Mushroom mode.

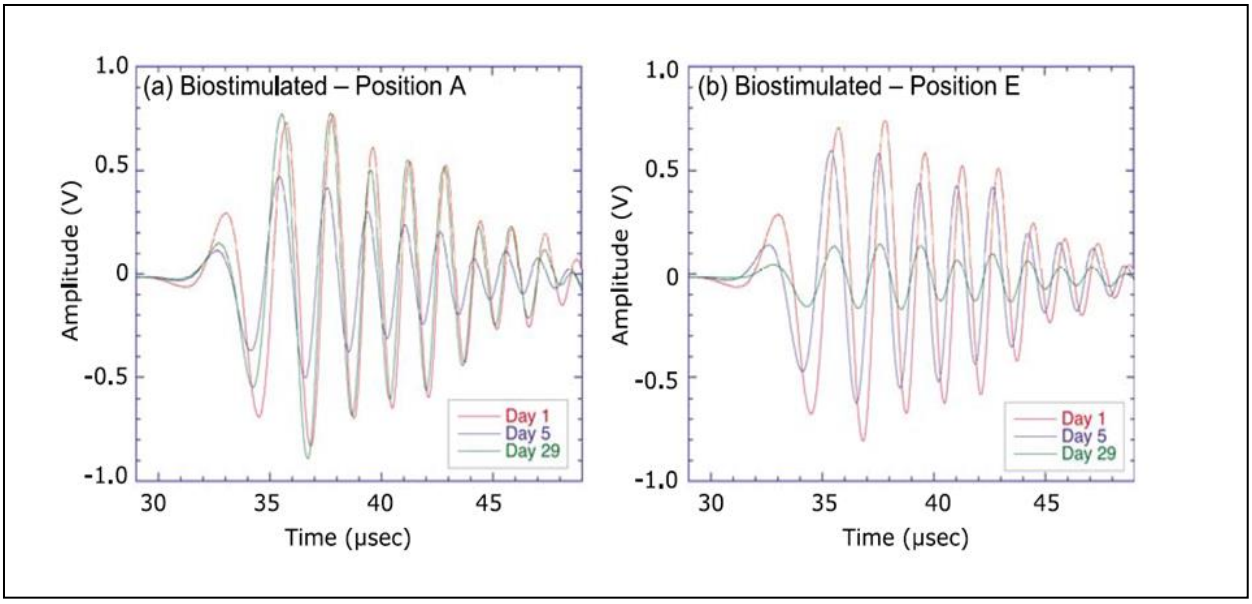

Figure 19.Transmitted compressional signals from the biostimulated column for days 1, 5, and 29 of the experiment for (a) position A and (b) position E (Davis et al., 2010).

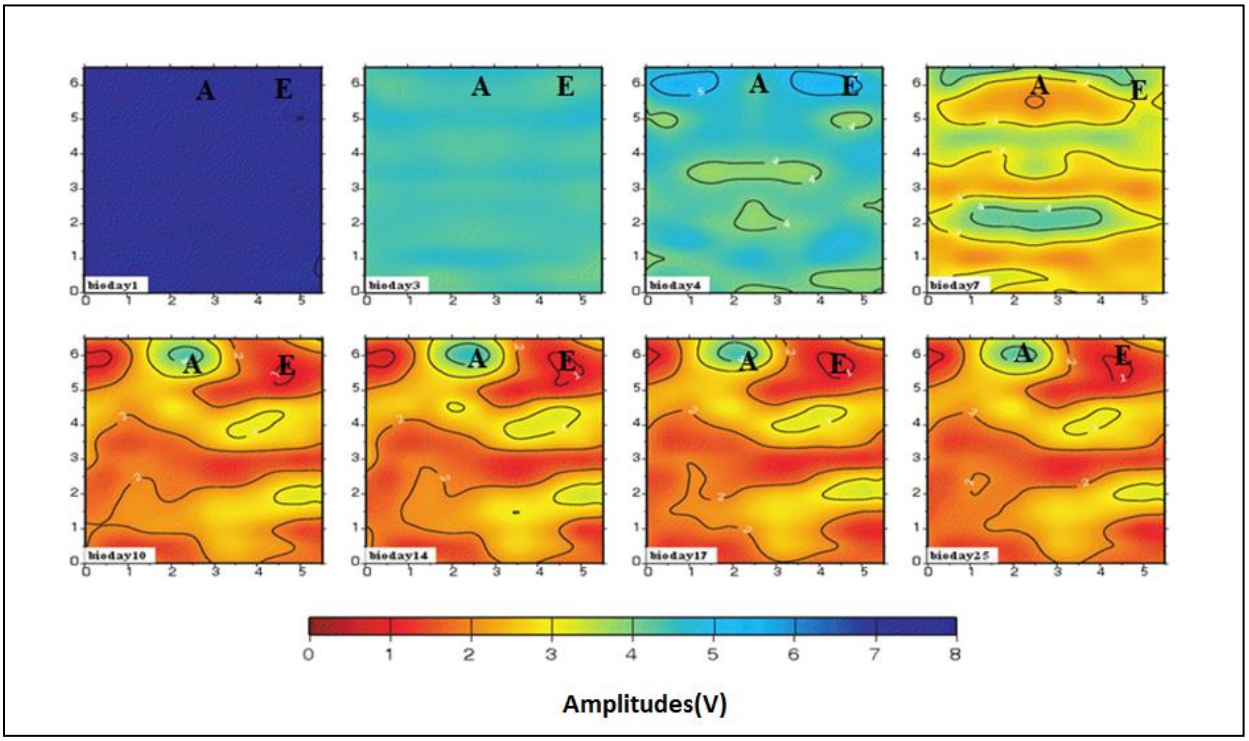

Figure 20. 2D amplitudes tomography maps for biostimulated data: (A) positioned of increased amplitude,(E) position of decrease amplitude.

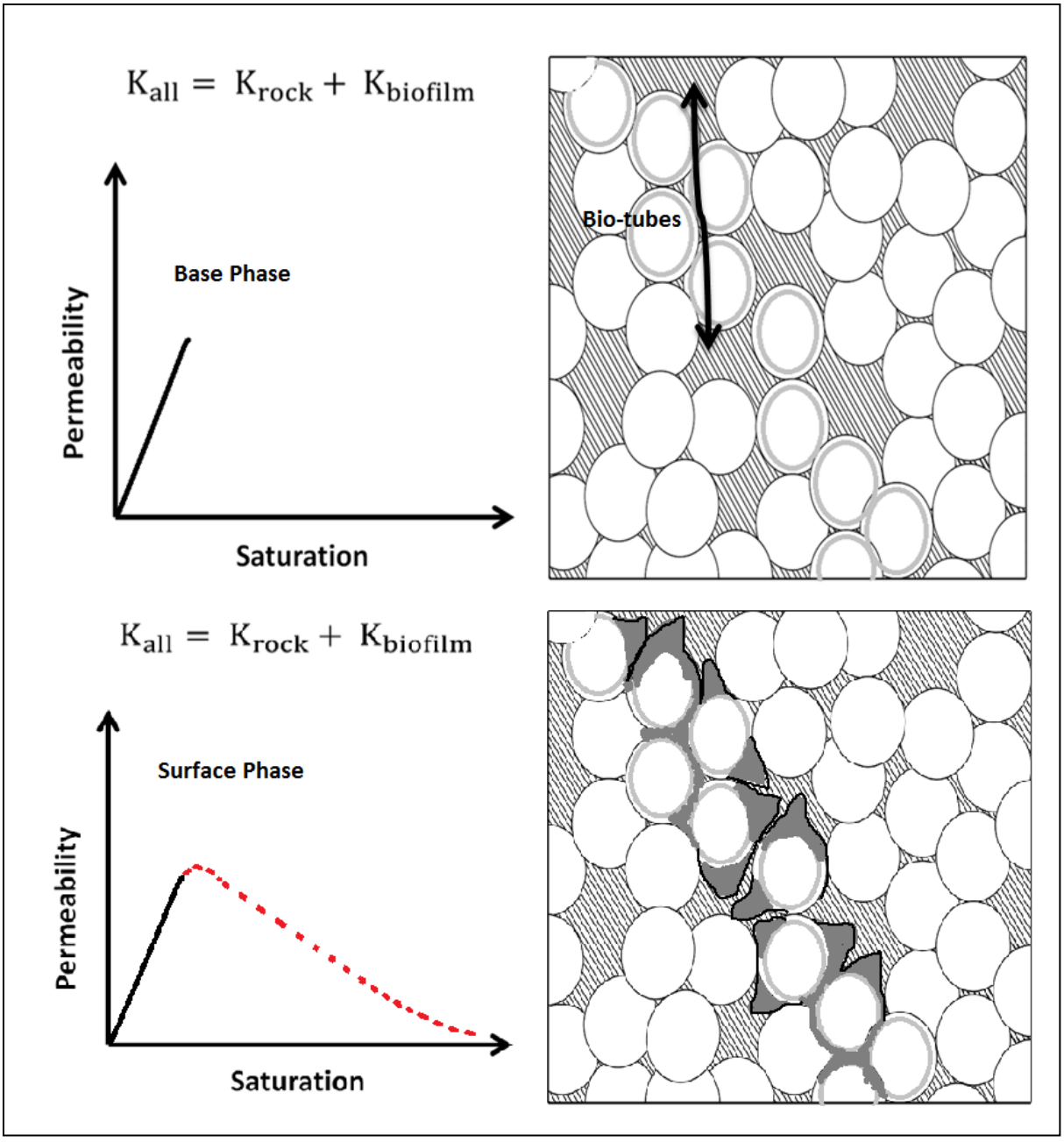

Figure 8.Permeability alterations due to microbial growth: Base phase where bio-tubes are created as thin layers to transmit fluids, Surface phase where the bio-tubes are blocked to reduce permeability and the porosity as well.

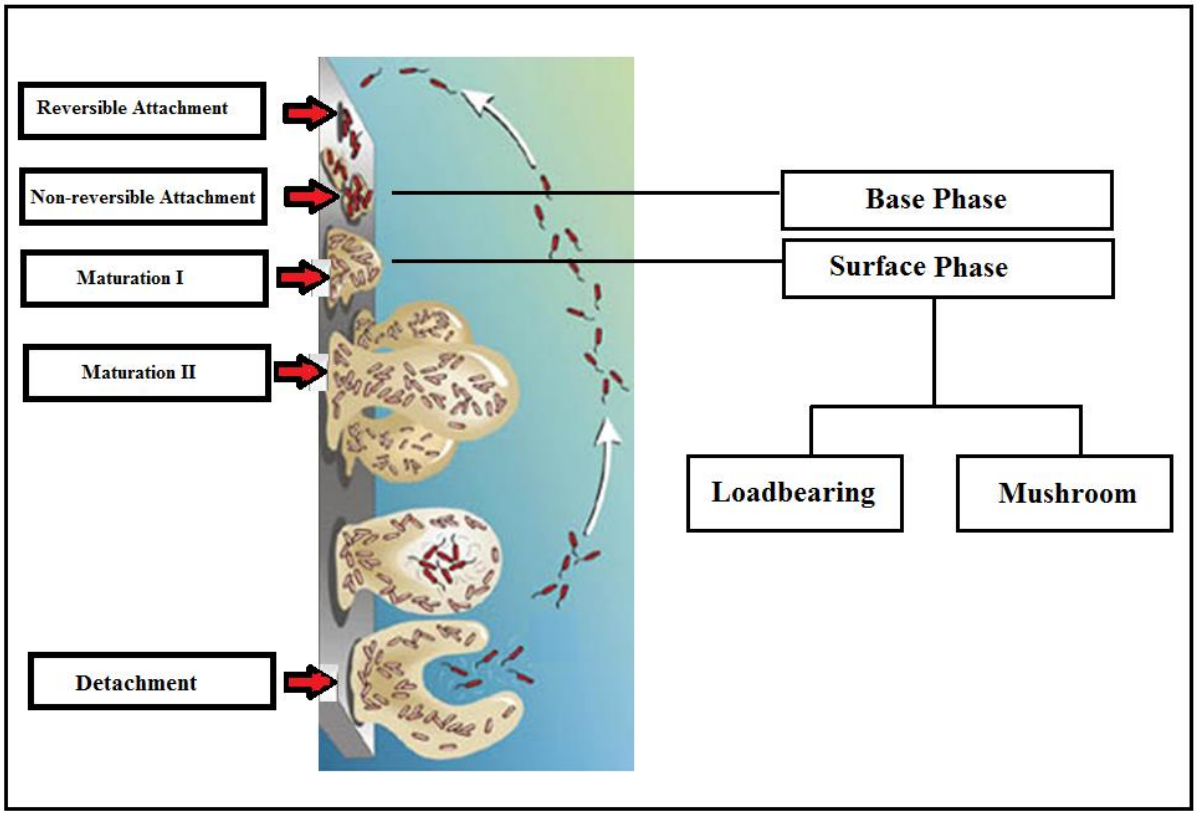

Figure 22. The relation between the biofilm development stages and the rock physics biofilm growth styles models.

VITA

Fathiya Mohammed Al- Hadhrami

Candidate for the Degree of

Master of Science

Thesis: ROCK PHYSICS MODELS FOR CONSTRAINING QUANTITVE INTERPRETATION OF ULTRASONIC DATA FOR BIOFILM GROWTH AND DEVELOPMENT

Major Field: Geology

Biographical:

Education:

Completed the requirements for the Master of Science in Geology at Oklahoma State University, Stillwater, Oklahoma in May, 2013.

Completed the requirements for the Bachelor of Engineering in Petroleum and Natural gas Engineering PNGE at University of Sultan Qaboos, Muscat, Sultanate of Oman in 2009.

Professional Memberships:

Member of the Society of Exploration Geophysicists (SEG)
Member of the American Association of Petroleum Geologists (AAPG).
Member of American Geophysical Union (AGU)
Member of Oklahoma Geological Society (OGS)